Vibrio parahaemolyticus quorum sensing controls phage VP882 transmission

Molly R. Sargen[1] and Bonnnie L. Bassler[1,2,3,*]

[1]Department of Molecular Biology, Princeton University, Princeton, New Jersey, United States of America

[2]Howard Hughes Medical Institute, Chevy Chase, Maryland, United States of America

[3]Lead contact

*Correspondence: bbassler@princeton.edu

Keywords: phage receptor, quorum sensing, superinfection, lysogeny

Abstract

Quorum sensing is a communication process bacteria use to orchestrate collective behaviors. Some temperate phages monitor bacterial quorum-sensing cues to track the abundance of vicinal host cells. Quorum-sensing-responsive phages can preferentially undertake lytic replication at high cell density, presumably maximizing transmission. If nearby host cells are lysogens, infections initiated by released virions could be nonproductive due to homoimmunity or superinfection exclusion, posing a conundrum for temperate phages. We define host and phage components influencing transmission of the quorum-sensing-responsive phage VP882 in *Vibrio parahaemolyticus populations*. Phage VP882 uses the K-antigen of serotype O3:K6 as its receptor. Host cells prevent phage attachment via quorum-sensing-controlled export of polysaccharides that shield the K-antigen from the phage at high cell density. Phage VP882 can superinfect and superlysogenize *V. parahaemolyticus*, overcoming the challenge of detecting whether or not potential hosts are lysogens. Following superlysogenization, recombination of phage genomes can occur possibly promoting genome diversification.

Introduction

Temperate phages alternate between lytic and lysogenic lifestyles[1]. When a phage is lytic, it replicates, kills its current host cell, and spreads to new cells. During lysogeny, the phage establishes a stable relationship with its host and is transmitted vertically as a prophage. Transitioning between lytic and lysogenic lifestyles enhances phage reproductive success by maximizing the potential for transmission[2]. Theory and experimental evidence suggest that phage transmission through the lytic route is often favored when susceptible hosts are abundant while lysogeny is preferred when potential new hosts are rare[3,4]. Quorum sensing (QS) is a cell-to-cell communication process in which bacteria produce, release, and detect extracellular signal molecules called autoinducers. QS enables bacteria to orchestrate collective behaviors[5]. Some temperate phages can monitor host QS autoinducers, allowing them to estimate host cell abundance and launch the lytic cycle at high cell density when many host cells are present[6,7].

A conundrum all temperate phages face when launching the lytic cycle is whether host cells in the vicinal community are already infected or not. Encountering bacteria that are already lysogens is often a dead-end for a phage because the lytic repressor produced from the genome of the resident lysogenic phage suppresses transcription from the newly infecting phage[8,9]. This process is known as homoimmunity and is protective for both the bacterial host and the resident prophage[10]. In other cases, prophages encode superinfection exclusion mechanisms that prevent infection of already lysogenized cells[11,12]. Superinfection immunity often occurs through alteration of the expression or function of the phage receptor on the host cell surface[13–16]. Superinfection exclusion protects lysogenic host cells and, unlike in the case of homoimmunity, also preserves the population of free phage virions so they are available to infect naïve hosts[17]. Homoimmunity and superinfection exclusion mechanisms potentially threaten the reproductive success of QS-responsive prophages that launch their lytic cycles at high cell densities.

Phage VP882, the first phage discovered to surveil a host QS autoinducer, infects the pathogen *Vibrio parahaemolyticus*. *V. parahaemolyticus* has two QS systems (Figure 1). First, the VqmA-VqmR QS pathway is controlled by the DPO autoinducer[18]. At high cell density, the VqmA transcription factor binds DPO, and the DPO-VqmA complex activates expression of *vqmR* encoding the VqmR small RNA (sRNA). VqmR promotes expression of genes required for group behaviors. Second, the LuxO-driven QS cascade is responsive to three autoinducers that are detected by three membrane bound receptors and, via a phosphorylation-dephosphorylation cascade, the receptors modulate the activity of the LuxO transcription factor[5]. At low cell density, LuxO is phosphorylated and it controls a regulon underpinning individual behaviors. At high cell density, LuxO is dephosphorylated, and under this condition, the regulon responsible for group traits is enacted.

The life cycle of phage VP882 is influenced by both the *V. parahaemolyticus* VqmA-VqmR[19] and LuxO QS systems[6,20], both promoting lytic replication at high host cell densities. Specifically, the phage VP882-encoded $VqmA_{Phage}$ receptor binds DPO[21] and DPO-$VqmA_{Phage}$ activates transcription of *qtip* encoding Qtip, a small protein anti-repressor that sequesters and inactivates cI, the phage VP882 lytic repressor[13]. Via an undefined mechanism, at high cell density, signaling through the LuxO QS system increases phage VP882 lytic gene transcription[20] favoring lytic replication over lysogeny[23].

If or how phage VP882 gauges the susceptibility of potential new host cells and whether hommoimmunity or superinfection exclusion occurs have not been investigated. Toward an understanding of those features, here we define factors that influence phage VP882 transmission. We identify the receptor of phage VP882 as the O3:K6 K-antigen that is specific to its host strain. We show that phage access to the O3:K6 K-antigen is controlled by LuxO-directed QS regulation of a transport system responsible for export of polysaccharides that shield the K-antigen. QS-mediated derepression of the genes encoding the transport system at high cell density prevents phage VP882 adsorption and infection. We demonstrate that phage VP882 does not encode a superinfection exclusion mechanism, so *V. parahaemolyticus* cells that are lysogenic for phage VP882 can be infected by virions released from neighboring cells. Following superinfection, DNA

from newly infecting phages can recombine with the resident phage genome resulting in superlysogenic conversion. We propose that QS-driven host superinfection via reliance on a specific K-antigen receptor could foster phage VP882 genomic diversification in lysogenic *V. parahaemolyticus* populations.

Results

The O3:K6 K-antigen is the phage VP882 receptor in *V. parahaemolyticus*

A primary determinant of phage transmission concerns the ability of phage to attach to host cells. In our continuing effort to define mechanisms that enable phage VP882 to propagate and to connect those mechanisms to its capability to surveil host QS, we investigated phage VP882 host range by identifying the *V. parahaemolyticus* phage receptor that enables infection. To do this, we performed transposon mutagenesis on *V. parahaemolyticus* 882, the natural host of phage VP882, that had been cured of the phage. We infected the pool of transposon insertion mutants with phage VP882 and isolated colonies that were not killed (Figure 2A). The notion was that surviving mutants were resistant to phage VP882 infection. Complicating this simple premise is that phage VP882 is a temperate phage, so infection can result in either lytic replication or lysogenization. Thus, following mutagenesis and infection, some host cells that survived could have been lysogens. To overcome this issue, the strain we used for the transposon mutagenesis carried a plasmid harboring arabinose-inducible *q* (denoted pBAD-*q*)[23]. Q is the phage VP882 activator of lytic gene expression. Consequently, the addition of arabinose to the surviving cells induced the lytic program in lysogens, thereby killing those cells. Presumably, this strategy resulted in survival of only *V. parahaemolyticus* 882 mutants resistant to phage VP882 infection (Figure 2A).

We screened surviving colonies for phage VP882 genes using PCR to ensure that the isolated mutants were phage-free. All phage-free mutants had acquired a translucent colony morphology that differed from that of the *V. parahaemolyticus* 882 parent, suggesting a modification to the cell surface (Figure S1A). Indeed, phage VP882 could not adsorb to nor form plaques on these mutants (Figure 2B and C, respectively; panel C shows one representative mutant). We sequenced the transposon insertion sites in 19 of these mutants. All of the insertions mapped to the K-antigen/capsule locus (*VP0215-VP0237*)[24] suggesting that this surface polymer could be the phage VP882 receptor (Figure 2D, Table S1). We generated in-frame deletions of *VP0230* (encoding a glycosyltransferase) and *VP0235* (encoding an epimerase) in the *V. parahaemolyticus* 882 chromosome and verified by adsorption and plaque assays that the phage could not adsorb nor propagate (Figure 2E and F, respectively), and identical to the original transposon insertion mutants, the deletion strains displayed the translucent colony morphology (Figure S1B; Δ*VP0235* is shown as the example). Some phages can use multiple host receptors to infect. To test whether phage VP882 might have such a capability, we assessed whether lysogenization of the *V. parahaemolyticus* Δ*VP0235* mutant occurred after extended incubation with a variant of phage VP882 carrying chloramphenicol resistance (denoted VP882$^{gp38::\mathrm{Cm}}$). *gp38* encodes a phage VP882 accessory gene[25] and elimination of it does not affect phage VP882 lysis of host cells (Figure S1C). This approach yielded no chloramphenicol resistant lysogens indicating that the *V. parahaemolyticus* K-antigen is the receptor for phage VP882 (Figure S1D).

Our identification of the K-antigen as the determinant of phage VP882 infectivity suggested that phage VP882 may specifically infect *V. parahaemolyticus* strains of the O3:K6 serotype, the serotype of its *V. parahaemolyticus* 882 host. To test this possibility, we screened our collection of *V. parahaemolyticus* isolates for susceptibility to phage VP882 infection by plaque assay. While not all of the serotypes of our isolates have been reported, phage VP882 formed plaques exclusively on isolates classified as serotype O3:K6 (Figure 2G and H; we discuss the differences in the extent of plaquing in the next section). Verifying this finding, only *V. parahaemolyticus* O3:K6 isolates produced chloramphenicol resistant colonies following infection with phage VP882$^{gp38::\mathrm{Cm}}$ (Figure S1E).

Notably, in the case of one of our O3:K6 serotype isolates, *V. parahaemolyticus* strain VP81, two colony morphologies were present in the stock obtained from ATCC (Figure S1F, designated col1 and col2 for colony type 1 and colony type 2). Colony type 1 had an opaque morphology resembling wildtype (WT) *V. parahaemolyticus* 882, and this *V. parahaemolyticus* VP81 morphotype was susceptible to phage VP882 infection and underwent lysis. By contrast, colony type 2 was translucent, resembling our *V. parahaemolyticus* 882 K-antigen mutants and was resistant to phage VP882 plaquing (Figure 2H and I). Whole genome sequencing of one colony of each morphotype revealed that the *V. parahaemolyticus* VP81 translucent colony 2 type possesses a frameshift mutation in *VP0235*, a gene in the K-antigen locus and a gene also identified in our transposon mutagenesis. Repair of this point mutation converted the colony from translucent to opaque (Figure S1F) and, moreover, restored the ability of phage VP882 to adsorb and plaque (Figure 2I and H, respectively). Together, our data support the model that the O3:K6 K-antigen is the receptor for phage VP882, and phage VP882 specifically attaches to and infects *V. parahaemolyticus* O3:K6 isolates because of its dependence on this antigen.

The particular features of *V. parahaemolyticus* O- and K-antigens that correspond to distinct serotypes have not been defined, so we cannot predict what K6 K-antigen moieties are recognized by phage VP882 nor how its relationship to the O3 O-antigen appendage affects phage VP882 recognition. Nonetheless, to preliminarily probe the basis for specificity of phage VP882 host range, we analyzed the O- and K-antigen loci in the genome sequences of our collection of *V. parahaemolyticus* strains. In agreement with our observations, all isolates designated O3:K6 harbor highly similar O- and K-antigen loci whereas these loci are markedly different in the genomes of non-O3:K6 strains. Few genes encoded in the K-antigen locus of *V. parahaemolyticus* O3:K6 can be identified in the other *V. parahaemolyticus* strains suggesting that their K-antigens are distinct. We conclude that the O3:K6 K-antigen is the essential receptor used by phage VP882.

LuxO-driven quorum sensing controls phage VP882 plaquing

Phage VP882 plaqued on all isolates of *V. parahaemolyticus* O3:K6 possessing genes encoding functional K-antigens. However, the extent of plaquing differed depending on the strain (Figure 2H). Specifically, when plated on *V. parahaemolyticus* 882 and *V. parahaemolyticus* VP47, phage VP882 readily formed large plaques at all phage concentrations. By contrast, on *V. parahaemolyticus* RIMD and *V. parahaemolyticus* VP81, phage VP882 formed plaques only at the highest concentration tested and the plaques were small. While *V. parahaemolyticus* VP47 and VP81 have not been well studied, one established difference between *V. parahaemolyticus* 882 and *V. parahaemolyticus* RIMD concerns their QS systems[20]. *V. parahaemolyticus* 882 harbors an

897 base pair deletion that eliminates the *vqmR* promoter, the *vqmR* coding sequence, and a portion of the non-coding region upstream of *vqmA*. Additionally, the *V. parahaemolyticus* 882 *luxO* gene (denoted $luxO_{882}$) harbors a 36 bp deletion that causes $LuxO_{882}$ to function as a phospho-mimetic. These mutations lock the respective QS systems into their low cell density modes. Given the connections between host QS and phage VP882 lifestyle transitions, we wondered whether these differences in QS capabilities could influence the differences in phage VP882 plaquing on the various host strains. To probe this possibility, we repaired one or both QS systems in *V. parahaemolyticus* 882 and assessed phage VP882 plaquing (Figure 3A and B). Restoration of VqmA-VqmR QS in *V. parahaemolyticus* 882 (denoted $vqmRA^{+}$) did not affect phage VP882 plaquing ability nor plaque size, and that was irrespective of the status of *luxO*. By contrast, when LuxO was restored to WT function (denoted $luxO^{+}$), phage VP882 made fewer and smaller plaques, similar to its behavior when plated on *V. parahaemolyticus* RIMD that possesses a functional LuxO (Figures 3A and 2H, respectively). Since plaque assays are performed at high cell density, this result indicated that LuxO-directed QS controls the ability of phage VP882 to plaque on *V. parahaemolyticus.* To verify this supposition, we replaced the native $luxO_{882}$ with either $luxO^{D61E}$ or $luxO^{D61A}$ that, respectively, lock *V. parahaemolyticus* into the low cell density and high cell density QS modes. Phage VP882 plaquing on *V. parahaemolyticus* 882 carrying $luxO^{D61E}$ was comparable to that on the parent *V. parahaemolyticus* 882 strain that carries the naturally low cell density locked $luxO^{882}$ variant. *V. parahaemolyticus* 882 carrying $luxO^{D61A}$ displayed phage VP882 plaquing comparable to that on strains with WT *luxO* (Figure 3A and B).

The plaquing phenotypes associated with the different *luxO* alleles mirrored the genotypes of the tested *V. parahaemolyticus* O3:K6 isolates. As mentioned, $LuxO_{882}$ locks *V. parahaemolyticus* 882 into the low cell density QS state, whereas LuxO in *V. parahaemolyticus* RIMD displays WT function and transitions from the low cell density to the high cell density QS state during growth. LuxO of *V. parahaemolyticus* VP47 harbors an M15R substitution. Analogous to *V. parahaemolyticus* 882 and all *V. parahaemolyticus* strains carrying $luxO^{D61E}$, *V. parahaemolyticus* VP47 was incapable of activating a P*luxC* reporter, the canonical QS-activated luciferase promoter that is used as the standard readout for QS function in vibrios[20] (Figure 3C). Thus, *V. parahaemolyticus* VP47 is locked in low cell density QS mode. Indeed, changing the arginine at position 15 back to methionine in *V. parahaemolyticus* VP47 LuxO restored density-dependent activation of P*luxC* (Figure 3C). Consistent with this finding, phage VP882 plaques only formed on *V. parahaemolyticus* VP47 carrying the repaired LuxO at high phage concentrations, and the plaques were smaller than those on the parent strain with the $luxO^{M15R}$ allele (Figure 3D). Together, our data show that signaling through the LuxO-controlled QS pathway dictates the robustness of phage VP882 plaquing on *V. parahaemolyticus*.

VPA1602-VPA1604 are quorum-sensing-controlled components that shield _V. parahaemolyticus_ from infection by phage VP882

We previously reported that LuxO QS signaling inhibits phage VP882 lysogenization at high cell density in *V. parahaemolyticus* RIMD[23]. Here, we show that a similar phenomenon occurs in *V. parahaemolyticus* 882, the natural host for phage VP882: higher numbers of lysogens formed during infection when the host is locked into low cell density QS mode than following infection of the host locked into high cell density QS mode (Figures 3E and S2A). One possibility was that these

206 differences stemmed from differences in the ability of the phage to adsorb to its *V.*
207 *parahaemolyticus* host when the host exists in the low and high cell density locked QS modes.
208 Indeed, 3-fold less phage VP882 adsorption occurred to *V. parahaemolyticus* 882 encoding WT
209 *luxO* and $luxO^{D61A}$ than to *V. parahaemolyticus* 882 harboring the $luxO_{882}$ and $luxO^{D61E}$ alleles
210 (Figures 3F and S2B). These data indicate that a QS-controlled factor influences phage VP882
211 entry into naïve host cells. We considered that QS might control production of the K-antigen.
212 However, examination of RNA-sequencing data from *V. parahaemolyticus* 882 carrying either WT
213 *luxO*, $luxO_{882}$, $luxO^{D61E}$, or $luxO^{D61A}$ showed no significant differences in K-antigen transcript levels
214 (Figure S3A)[20]. Thus, we suspected that some other component regulated by LuxO exists in *V.*
215 *parahaemolyticus* strains and affects phage VP882 adsorption and entry.

216 To identify the putative factor that inhibits phage VP882 entry into *V. parahaemolyticus* 882, we
217 carried out a selection for *V. parahaemolyticus* 882 mutants displaying enhanced phage VP882
218 adsorption and entry at high cell density. Specifically, we generated a transposon mutant library
219 in *V. parahaemolyticus* 882 carrying $luxO^{D61A}$, infected it with phage $VP882^{gp38::Cm}$, and selected
220 chloramphenicol resistant lysogens. Sequencing of the transposon insertion sites in 54 lysogens
221 (Table S2) revealed that nearly all insertions resided in unique locations. Most interesting to us
222 were four insertions in or near the *VPA1602-4* operon. *VPA1602-4* are predicted to encode
223 homologs of Wza, Wzb, and Wzc. Wzabc proteins are involved in export of extracellular
224 polysaccharides such as those required for the *Escherichia coli* Group 1 capsules[26]. Deletion of
225 this operon in *V. parahaemolyticus* strains of the O3:K6 serotype have no effect on K-antigen
226 production[24], so we hypothesized that VPA1602-4 are involved in the production and export of a
227 polysaccharide that blocks access of phage VP882 to the K-antigen. Indeed, deletion of *VPA1602-*
228 *4* restored the ability of phage VP882 to adsorb to *V. parahaemolyticus* 882 $luxO^{D61A}$ (Figure 4A).
229 Furthermore, adsorption to all tested *V. parahaemolyticus* 882 strains required the K-antigen
230 including in the absence of *VPA1602-4* (Figure 4A). Consistent with our findings, transcription of
231 *VPA1602-4* is activated at high cell density (Figure S3B and C)[20] and the homologous operon in
232 *Vibrio harveyi* (*VIBHAR_06665-7*) is repressed at low cell density[27]. These patterns, coupled with
233 our data showing that mutation of *VPA1602-4* promotes phage VP882 adsorption to *V.*
234 *parahaemolyticus* 882 $luxO^{D61A}$, suggest that VPA1602-4 are involved in production and export of
235 a polysaccharide that blocks phage access to the K-antigen.

236 The export substrates of VPA1602-4 in *V. parahaemolyticus* are undefined. Table S2 shows that,
237 in the above screen, we also isolated singleton transposon insertions in genes involved in
238 polysaccharide biosynthesis pathways (*galU, nagE,* and *neuC*) that enabled phage VP882 entry.
239 We considered that these additional genes could provide clues concerning the polysaccharide
240 produced by VPA1602-4. However, deletion of these genes had no effect on phage VP882
241 adsorption, so we conclude that they are not required for production of the polysaccharide
242 exported by VPA1602-4 (Figure S3D). We did not investigate the functions of these genes further.
243 Possibly, the VPA1602-4 system exports multiple substrates that affect K-antigen access to phage
244 VP882 explaining why we did not identify the polymer in the transposon screen.

245 Deletion of *VPA1602-4* enabled phage VP882 to adsorb to all *V. parahaemolyticus* 882 hosts
246 irrespective of QS genotype (Figures 3A and S3E). Restoration of phage VP882 adsorption via
247 elimination of *VPA1602-4* also rescued the ability of phage VP882 to lysogenize each *V.*

248 *parahaemolyticus* strain under study to near equivalent levels (Figures 3B and S3F) while having
249 no discernable effect on phage VP882 plaquing (Figure S3G). These results indicate that the major
250 determinant of the LuxO QS effect on phage VP882 lysogenization of *V. parahaemolyticus* 882 is
251 through suppression of phage VP882 virion adsorption to host cells and not via effects on the
252 subsequent lysis-lysogeny decision. Thus, LuxO QS regulation of *VPA1602-4* is a host mechanism
253 that influences the spread of phage VP882 in *V. parahaemolyticus* O3:K6 populations by shielding
254 the K6-antigen (Figure 4C).

255 **Superinfection of *V. parahaemolyticus* phage VP882 lysogens leads to phage VP882 genome**
256 **recombination**

257 The above data define how LuxO QS influences phage VP882 transmission to naïve hosts. An
258 outstanding question remained regarding the fate of phage VP882 virions released into a
259 population of QS *V. parahaemolyticus* O3:K6 cells in which virions are likely to encounter hosts
260 that are already lysogens. Superinfection exclusion, via alteration of the expression or function of
261 the phage receptor, is often employed by lysogens to prevent re-infection[12]. We wondered if
262 phage VP882 encodes a superinfection exclusion mechanism that would prevent it from infecting
263 lysogens.

264 We examined superinfection by plaque assay. Phage VP882 did not form plaques when plated on
265 *V. parahaemolyticus* 882 that was already lysogenic for phage VP882 (Figure 5A). However, in this
266 experiment, homoimmunity, mediated by the resident phage VP882 cI repressor of lysis, could
267 have prevented infecting phages from initiating the lytic replication program necessary for plaque
268 formation even if the virions had adsorbed to and infected lysogens. By exploiting a phage VP882
269 lysogen that cannot produce functional virions, we found that phage VP882 can indeed adsorb to
270 *V. parahaemolyticus* 882 cells that are already lysogenized with phage VP882 (Figure 5B). Thus,
271 no superinfection exclusion mechanism prevents adsorption of phage VP882 virions to
272 lysogenized hosts.

273 Following adsorption to *V. parahaemolyticus* 882 lysogens, we wondered whether injection of
274 the phage genome occurred. To probe this issue, we assessed whether infection of *V.*
275 *parahaemolyticus* 882 lysogens with phage VP882$^{gp38::\mathrm{Cm}}$ generated chloramphenicol resistant
276 colonies. Indeed, chloramphenicol resistant lysogens were produced at levels similar to those
277 resulting from infection of *V. parahaemolyticus* 882 that had been cured of phage VP882 (Figure
278 5C). Thus, phage VP882 virions can both attach to lysogenic cells and inject their genomes. We
279 call new lysogens, which originate from existing *V. parahaemolyticus* 882 phage VP882 lysogens
280 and acquire DNA from an infecting phage VP882, superlysogens.

281 The influence of QS on phage VP882 lysogenization of *V. parahaemolyticus* 882 via regulation of
282 *VPA1602-4* was maintained during superinfection. Specifically, lysogens of *V. parahaemolyticus*
283 882, which is naturally locked into the low cell density QS mode, were converted to
284 chloramphenicol resistant superlysogens at a higher frequency than were *V. parahaemolyticus*
285 882 lysogens locked into high cell density QS mode (Figure 5C). Deletion of *VPA1602-4* restored
286 lysogenization of both the phage-cured and lysogenized high cell density locked QS *V.*
287 *parahaemolyticus* 882 strains to the levels of the corresponding *V. parahaemolyticus* 882 low cell
288 density locked cured and lysogenic strains (Figure 5C). These results indicate that LuxO regulation

289 of *VPA1602-4* occurs in *V. parahaemolyticus* 882 lysogens and non-lysogens, and thus, host QS
290 status dictates the outcome of phage VP882 superinfection by affecting phage entry.

291 The transfer of chloramphenicol resistance following phage VP882$^{gp38::Cm}$ infection of *V.*
292 *parahaemolyticus* 882 lysogens indicates that lysogens acquire superinfecting phage DNA. We
293 considered the fates of the resident and superinfecting phage genomes during phage VP882
294 superinfection and superlysogenization. Phage VP882 is a linear plasmid-phage that exists in
295 multiple copies per cell. Superinfection could result in a heterogeneous population of phage
296 genomes. Alternatively, superinfection could result in exchange of the existing phage genomes
297 with the infecting phage genome. Finally, superinfection could result in recombination of resident
298 and infecting phage genomes. To test which possibility occurs, we infected *V. parahaemolyticus*
299 882 lysogens with phage VP882 harboring a chloramphenicol marker in an intergenic region near
300 the 3' terminus of the phage genome (denoted VP882$^{gp7\text{-}1\text{intergenic::Cm}}$). We investigated whether
301 the chloramphenicol resistance marker was maintained in lysogens that acquired gentamicin
302 resistance during superinfection with phage VP882 carrying a gentamicin resistance marker in
303 *gp38* (denoted VP882$^{gp38::Gm}$). *gp38* is located near the center of the phage genome (Figure S4).
304 We reasoned that if the phage genomes co-exist following superinfection, all superlysogens
305 would be both gentamicin and chloramphenicol resistant. By contrast, if the phage genomes were
306 exchanged, all superlysogens would exhibit only gentamicin resistance. Third and lastly, if
307 recombination of phage genomes occurred, some superlysogens would be exclusively gentamicin
308 resistant and some would display resistance to both gentamicin and chloramphenicol.
309 Importantly, our method only allows us to detect superlysogenization events that result in the
310 acquisition of gentamicin resistance, we cannot detect events in which gentamicin is acquired
311 and then lost following recombination (Figure S4). The third possibility occurred (Figure 5D)
312 suggesting that recombination occurs between the resident and newly infecting phage genomes.
313 Deletion of *recA*, encoding the recombinase required to initiate homologous recombination, did
314 not affect the level of lysogenization of naïve *V. parahaemolyticus* 882 nor of *V. parahaemolyticus*
315 882 lysogenized with phage VP882 (Figure 5E). However, *V. parahaemolyticus* 882 Δ*recA* lysogens
316 carrying VP882$^{gp71\text{intergenic::Cm}}$ did not yield doubly antibiotic-resistant superlysogens when
317 infected with phage VP882$^{gp38::Gm}$ (Figure 5D); all of the colonies that had acquired gentamicin
318 resistance had lost chloramphenicol resistance. Furthermore, infection of *V. parahaemolyticus*
319 882 lysogens carrying VP882$^{gp38::Cm}$ with phage VP882$^{gp38::Gm}$ did not yield doubly antibiotic-
320 resistant lysogens (Figure 5D). Thus, when recombination that places both antibiotic resistance
321 markers onto the same phage genome is prevented or is not possible, the superlysogens acquire
322 the entire genome of the infecting phage. Together, these results suggest that only one variant of
323 the phage VP882 genome is maintained in *V. parahaemolyticus* and, during superinfection,
324 recombination occurs between the infecting and resident phage genomes to enable this
325 outcome.

326 To confirm the above findings, we tested whether all the phage genomes in a *V. parahaemolyticus*
327 882 superlysogen were identical or not. To do this, we used PCR amplification of the loci
328 containing the resistance cassettes in doubly-antibiotic resistant *V. parahaemolyticus* 882
329 superlysogens (Figure S4). The logic is if only one phage genome is present, PCR amplification
330 spanning either the *gp38* or the *gp71*-intergenic locus will yield a single PCR product, while if two
331 phage genomes are maintained, PCR amplification should yield two PCR products corresponding

332 to the allele containing and lacking the resistance marker. PCR amplification yielded one product
333 for each locus, and the product size corresponded to the phage with the resistance cassette in
334 each locus (Figure 5F). Additionally, both gentamicin and chloramphenicol resistance were
335 maintained when these superlysogens were grown in the absence of antibiotic selection. This
336 result indicated that the markers were linked and could not independently segregate over
337 multiple generations. These data support our model that recombination occurs between the
338 infecting and resident phage genomes during superinfection and only one variant of the phage
339 genome is maintained.

340 **Discussion**

341 Phage VP882 engages with both QS systems of its host *V. parahaemolyticus* and funnels the
342 information it garners into control of transitions between lysogeny and lytic replication (Figure 1).
343 Monitoring host QS enables phage VP882 to favor transitioning from lysogeny to lysis at high host
344 cell densities. Presumably, skewing transitions in this direction increases the frequency of
345 released phage VP882 virions encountering new host cells. An outstanding question was whether
346 those encounters are productive given that monitoring host QS cues does not provide the phage
347 information concerning whether or not nearby host cells are already lysogens. Irrespective of
348 encounter frequency, populations of hosts that are predominantly lysogens could restrict phage
349 VP882 transmission if resident VP882 phages deploy homoimmunity or superinfection exclusion
350 mechanisms that block subsequent phage infection or propagation.
351
352 Here, we identify and characterize host components that influence transmission of phage VP882
353 in QS populations of *V. parahaemolyticus*. We identify the receptor used by phage VP882 as the
354 O3:K6 K-antigen that is specific to its host strain (Figure 2B-F). We show that phage access to the
355 O3:K6 K-antigen is controlled by LuxO-driven QS regulation of a transport system that exports
356 polysaccharides that shield the K-antigen from the phage at high cell density (Figure 4A and C).
357 We demonstrate that phage VP882 does not encode a superinfection exclusion mechanism, so *V.*
358 *parahaemolyticus* lysogens can be superinfected by virions released from neighboring cells
359 (Figure 5D). Our data demonstrate that following superinfection, DNA from newly infecting phage
360 genomes can be maintained in the entirety or can recombine with the resident phage genome
361 resulting in superlysogenic conversion (Figure 5D and F). Thus, phage VP882 avoids unproductive
362 encounters with already lysogenized hosts. We propose that, together, superinfection and phage
363 genome recombination promote phage VP882 spread and genomic diversity in lysogenic *V.*
364 *parahaemolyticus* populations.
365
366 Phage VP882 could employ the specific K-antigen receptor to ensure transmission to similar hosts
367 to which the phage arrives well-adapted. As a plasmid-phage, and we have experimentally
368 demonstrated this trait previously[6], phage VP882 can persist in, replicate in, and lyse a wide
369 variety of very distantly related/unrelated bacterial species because its RepA module is sufficient
370 for plasmid maintenance and does not require a specific site in the host genome for the phage to
371 lysogenize. However, the narrow distribution of the O3:K6 receptor guarantees that, in natural
372 settings, phage VP882 exclusively infects *V. parahaemolyticus* strains of that serotype.
373 Interestingly, both the LuxO and VqmR-VqmA systems that influence phage VP882 lifestyle
374 transitions are only present in *vibrio spp*[5,6]. Rigid receptor-specificity could serve as a gate-keeping

375 mechanism to ensure the prophage receives the benefits of detecting and responding to the
376 multiple host QS signals by restricting infection to only similar *V. parahaemolyticus* strains.
377 Recently, VP882-like plasmid-phages have been discovered that reside in other bacterial
378 species[25]. It will be fascinating to learn if they too use specific receptors that constrain host range
379 to hosts to which they are likewise highly adapted.
380
381 While QS plays an overarching role in interactions between phage VP882 and its *V.*
382 *parahaemolyticus* host, here, we find that QS also drives host adaptation to the phage.
383 Specifically, at high cell density, LuxO-QS activates production of a polysaccharide export system
384 that protects *V. parahaemolyticus* from phage VP882 adsorption and therefore, infection. In other
385 phage-bacterial systems, QS-controlled restriction of phage propagation is mediated by
386 alterations in phage receptor availability, via upregulation of CRISPR systems, and through control
387 of abortive infection mechanisms[28–31]. In the current case, we find that changes in phage VP882
388 adsorption do not alter phage VP882 lytic propagation but, rather, affect the ability of phage
389 VP882 to lysogenize its host. Clearly, additional QS-controlled mechanisms that modulate phage
390 VP882 activity exist in *V. parahaemolyticus* that, for example, contribute to differences in phage
391 VP882 plaquing when phage VP882 adsorption is equivalent among strains (Figure S3G).
392 Potentially, *V. parahaemolyticus* has evolved multiple strategies to counteract phage VP882 in
393 response to the phage's pervasive infective capability.
394
395 Rather than deploying a superinfection exclusion mechanism that diverts phage VP882 progeny
396 to infection of naïve hosts[12] or a mechanism that detects the abundance of lysogens or like phages
397 in the vicinal community[3], phage VP882 infects lysogens that already harbor phage VP882. While
398 phage VP882 does not propagate immediately following superinfection, as noted above, these
399 infection events are not unproductive, as the newly infecting phage DNA can be maintained in
400 the superinfected host. We propose that coupling surveillance of QS cues with superinfection is
401 especially beneficial to phage VP882 compared to phages that do not possess one or both of
402 these capabilities. First, lysis primarily occurs when many potential host cells are present and
403 infection or superinfection promotes phage transmission. Second, superlysogenization could
404 promote phage VP882 genetic diversity. Our data indicate that the primary outcome of
405 superlysogenization is that a single phage genome is maintained in the host. Consistent with our
406 notion that this process fosters genomic diversity, we demonstrate that, in many cases,
407 superinfection results in recombination between the resident and infecting phage genomes. We
408 detect these events in 1-5% of superlysogens (Figure 5D), but the frequency of recombination is
409 likely higher as only a subset of recombination events can be detected by our markers.
410 Superinfection resulting in either genome exchange or recombination potentially enhances the
411 spread of phage VP882 variants because genomes of variants with reduced fitness can be
412 replaced by genomes or portions of genomes from successfully replicating and successfully
413 superinfecting phages. The narrow host specificity phage VP882 displays via dependence on the
414 K6 antigen presumably increases the likelihood that, if virions encounter a lysogen that the virion
415 can infect, the resident phage genome will be similar enough to the newly infecting phage
416 genome for recombination to occur.
417

Together, our data reveal that phage VP882 transmission is influenced by both host and phage features that hinge on bacterial QS inputs. At high host cell density, phage VP882 lytic replication is stimulated by inputs from both QS systems of *V. parahaemolyticus* host cells[6,20]. Superinfection enables phage VP882 to overcome the challenge temperate phages face when they induce their lytic cycle in populations of lysogens. In this case, superinfection moreover ensures that phage VP882 can capitalize on its interception of bacterial QS cues. *V. parahaemolyticus* host cells "fight back" by restricting phage VP882 spread using QS-directed production of a receptor-shielding molecule, also at high cell density. Potentially, this host strategy could broadly defend against phage infection. In the context of our current work, the receptor-shielding mechanism tips phage VP882 lysogeny toward naïve host populations and conditions of low host abundance, both of which are non-optimal for phage VP882 to propagate and diversify. Thus, bacterial QS signaling underlies both host and phage behaviors that shape the outcomes of phage VP882 replication and host encounters. These dynamics could differ for other phage-host pairs depending on the selection pressures germane to their specific environments and the mechanisms connecting phage processes to host QS signaling.

Acknowledgements

We are grateful to members of the Bassler laboratory for insightful discussions.

Funding

This material is based upon work supported by the Howard Hughes Medical Institute and the National Science Foundation (grant MCB-2508324) (B.L.B.). The funders had no role in study design, data collection and analysis, decision to publish, or preparation of the manuscript. Any opinions findings and conclusions or recommendations expressed in this material are those of the authors and do not necessarily reflect the views of the National Science Foundation.

Author Contributions

Outlined the study: M.R.S and B.L.B.
Performed experiments: M.R.S
Analyzed data: M.R.S and B.L.B.
Interpreted data: M.R.S and B.L.B.
Wrote manuscript: M.R.S and B.L.B.

Declaration of Interests

The authors declare no competing interests.

Lead contact

Requests for further information and reagents may be directed to and will be fulfilled by the lead contact, Bonnie L. Bassler (bbassler@princeton.edu).

Materials availability

All plasmids in this study are available from the lead contact upon request.

Data and code availability

462 No sequencing or custom code is included in this manuscript.

463 **Figure Legends**
464

465 **Figure 1: Phage VP882 engages with both host quorum-sensing systems**

466 Both the *V. parahaemolyticus* VqmA-VqmR and LuxO QS systems influence the life cycle of phage
467 VP882 by both promoting lytic replication at high host cell densities. See text for details.

468

469 **Figure 2: The O3:K6 K-antigen is the phage VP882 receptor in *V. parahaemolyticus***

470 A) Diagram of transposon screen to identify genes encoding the phage VP882 receptor. B)
471 Quantitation of phage VP882 adsorption. Bacteria were incubated with phage VP882 lysate (final
472 MOI 10^{-3}-10^{-4}) for 20 min. Bacteria and adsorbed phage particles were separated from
473 unabsorbed (free) phage by centrifugation. Free phage were quantified by plaque assay on *V.*
474 *parahaemolyticus* cured of phage VP882. Percent free phage was calculated relative to a sample
475 lacking bacteria, and the value from that experiment was set to 100%. C) Phage VP882 plaque
476 formation on the designated strains. Ten-fold serial dilutions of phage VP882 lysate (starting at
477 10^{-8}-10^{-9} PFU/mL) were spotted on lawns of the indicated *V. parahaemolyticus* strains embedded
478 in 0.5% LB top agar overlaid onto 1.5% LB agar. Plaques were quantified after 16-20 h of
479 incubation at 37 °C. D) Diagram of *V. parahaemolyticus* 882 O- and K-antigen loci. The K-antigen
480 is encoded by *VP0215*-*VP0237* (blue). Transposon insertion sites are depicted as vertical lines
481 below genes. Black and red indicate insertions on the + and – strands, respectively. Genes shown
482 in black are markers that commonly flank O- and K-antigen loci in *V. parahaemolyticus* (from left
483 to right *coaD*, *gmhD*, and *rjg*). E and F) As in B and C, respectively, for the designated strains. G)
484 Table reporting *V. parahaemolyticus* serotypes, when known. + indicates plaques detected in 3
485 biological replicates. - indicates no plaques detected. H) As in C for the designated strains. col1
486 and col2 denote the translucent and opaque morphotypes, respectively. *VP0235+* indicates repair
487 of the frameshift in *VP0235*. I) As in B for the designated strains. In B, E, and I, data are presented
488 as means of 3 biological replicates and error bars denote SEMs. Significance was determined by
489 one-way ANOVA with Tukey's test for multiple comparisons to establish adjusted p-values. In C, F,
490 and H, a representative image from 3 biological replicates is shown.

491

492 **Figure 3: LuxO-driven quorum sensing controls phage VP882 infection**

493 A) Phage VP882 plaque formation on the designated phage-free strains, as in Figure 2C. B)
494 Quantification of plaque formation of phage VP882 on the designated strains from panel A.
495 Shown are the log differences in scores for phage VP882 clearance following infection of each
496 strain compared to that for infection on *V. parahaemolyticus* 882 (see Methods). C)
497 Bioluminescence output from P*luxC*-*luxCDABE* after 300 min of growth in LM at 30 °C of the
498 designated strains. Relative light units (RLU) are bioluminescence normalized to OD_{600}. D) Phage
499 VP882 plaque formation on the designated strains as in Figure 2C. E) Quantitation of phage
500 VP882$^{gp38::Cm}$ lysogens following infection of the designated phage-free strains (MOI 10^{-5}-10^{-6}). F)
501 Quantitation of phage VP882 adsorption as in Figure 2B. In B, C, E, and F, data are presented as

means of 3 biological replicates and error bars denote SEMs. Significance was determined by one-way ANOVA with Tukey's test for multiple comparisons to determine adjusted p-values as indicated. In B, the reported p-values above each bar specify comparisons to *V. parahaemolyticus* 882. In A and D, a representative image from 3 biological replicates is shown.

Figure 4: VPA1602-VPA1604 are quorum-sensing-controlled components that shield *V. parahaemolyticus* from infection by phage VP882

A) Quantitation of phage VP882 adsorption as in Figure 2B. B) Quantitation of phage VP882 lysogens as in Figure 3E. Data are presented as means of 3 biological replicates and error bars denote SEMs. Significance was determined by one-way ANOVA with Tukey's test for multiple comparisons to establish adjusted p-values. C) Diagram of *V. parahaemolyticus* K-antigen and the putative extracellular polysaccharide that shields it.

Figure 5: Superinfection of *V. parahaemolyticus* phage VP882 lysogens leads to phage VP882 genome recombination

A) Phage VP882 plaque formation as in Figure 2C. A representative image from 3 biological replicates is shown. B) Quantitation of phage VP882 adsorption as in Figure 2B. The phage used for infection, phage VP882$^{\text{Ctr::Tn}5}$, does not produce functional virions that could interfere with quantitation. C-E) Quantitation of phage VP882 lysogens as in Figure 3E except that in panels D and E, phage VP882$^{gp38\text{::Gm}}$ was the infecting phage. In panel D, lysogens carried phage VP882$^{g71\text{-intergenic::Cm}}$. F) PCR products resulting from amplification of the *gp38* and *gp71*-intergenic loci in the resident and infecting phage VP882 genomes and doubly-resistant superlysogens from the experiment in Figure 5D. Diagrams depict the expected PCR product size for each locus in the resident phage (VP882$^{g71\text{-intergenic::Cm}}$, green) and the infecting phage (VP882$^{gp38\text{::Gm}}$, black). 12-18 colonies were assayed in 3 biological replicates, and a representative gel is shown. In B, C, D, and E, data are presented as means of 3 biological replicates and error bars denote SEMs. In B, significance was determined by an unpaired t-test. In C, D, and E significance was determined by one-way ANOVA with Tukey's test for multiple comparisons to establish adjusted p-values.

Figure S1: Phage VP882 only infects *V. parahaemolyticus* with the O3:K6 K-antigen

A and B) Colony morphologies of the designated phage-free *V. parahaemolyticus* 882 strains grown on LB agar at 37 °C for 16 h. C) Growth curves of *V. parahaemolyticus* 882 carrying phage VP882 or phage VP882$^{gp38\text{::Cm}}$ treated with mitomycin C (0.05 µg/mL). A representative of 2 biological replicates is shown. Each assay included 2 technical replicates. D) Quantitation of phage VP882$^{gp38\text{::Cm}}$ lysogens following infection of the designated phage-free strains, as in Figure 3E except that lysogenization was carried out for 16 h. E) Quantitation of phage VP882$^{gp38\text{::Cm}}$ lysogens as in Figure 3E. F) Colony morphologies of the designated phage-free strains grown on LB agar at 37 °C for 16 h. In A, B, and F, a representative image from 3 biological replicates is

540 shown. In C, D, and E, data are presented as means of 3 biological replicates and error bars
541 indicate SEMs. We note that in panel C, error bars are obscured by the symbols.

542

543 **Figure S2: VqmA-VqmR quorum sensing does not affect phage VP882 infection**

544 A) Quantitation of phage VP882 lysogens as in Figure 3E. B) Quantitation of phage VP882
545 adsorption as in Figure 2B. Data are presented as means of 3 biological replicates and error bars
546 indicate SEMs.

547

548 **Figure S3: *VPA1602-VPA1604* are controlled by the LuxO quorum-sensing system**

549 A) Heatmap showing quantitation of RNA-seq reads mapping to the *V. parahaemolyticus* K-
550 antigen locus for strains with the indicated QS genotypes after 4 h of growth in LM at 30 °C[20]. The
551 fraction of total reads aligning to each gene were normalized to the corresponding value for *V.*
552 *parahaemolyticus* 882. B) Quantitation of RNA-seq reads mapping to *VPA1602* from the
553 conditions described in A[20]. C) P*VPA1602-luxCDABE* output as in Figure 3C except measurements
554 were taken after 500 min. D and E) Quantitation of phage VP882 adsorption as in Figure 2B. F)
555 Quantitation of phage VP882 lysogens as in Figure 3E. G) Quantification of phage VP882 plaque
556 formation as in Figure 3B. For D-G, data are presented as means of 3 biological replicates and
557 error bars indicate SEMs. In C and D, significance was determined by one-way ANOVA with Tukey's
558 test for multiple comparisons to establish adjusted p-values.

559

560 **Figure S4: Phage VP882 genome recombination occurs during superlysogenization**

561 Diagram of phage VP882 genomes used to monitor recombination in the superinfection
562 experiments reported in Figure 4D and F.

563 **Methods**
564
565 **Bacterial strains, reagents, and growth conditions**
566 *Escherichia coli* strains were grown with aeration in Lysogeny Broth (LB-Miller, BD-Difco) at 37
567 °C. *V. parahaemolyticus* strains were grown with aeration in LM (LB with 2% NaCl) at 30 °C. Strains
568 used in the study are listed in Table S3. Unless otherwise noted, antibiotics were used at: 50
569 µg/mL kanamycin (GoldBio), 50 µg/mL polymyxin B (Sigma), 10 µg/mL chloramphenicol (Sigma),
570 and 30 µg/mL gentamicin (Sigma). Diaminopimelic acid (DAP, Sigma) was used at 100 µM. For
571 phage lysis and bioluminescent reporter assays, overnight cultures of *V. parahaemolyticus* strains
572 were diluted 1:100 into fresh LM containing antibiotics when appropriate. After 2 h of growth at
573 30 °C with aeration, cultures were diluted 1:100 into fresh medium with appropriate antibiotics
574 prior to being dispensed (200 µL/well) into 96 well plates (Corning Costar 3903). When needed,
575 0.05 µg/mL mitomycin C was added at the second dilution step. A BioTek Synergy Neo2 Multi-
576 Mode reader was used to measure OD_{600} and bioluminescence. Relative Light Units (RLU) are
577 bioluminescence divided by OD_{600}. P*luxC-luxCDABE* expression was measured at 300 min of
578 growth. P*VPA1602-luxCDABE* expression was measured at 500 min of growth.
579
580 **Cloning techniques**
581 All primers used for plasmid construction and qPCR, listed in Table S4, were obtained from
582 Integrated DNA Technologies. FastCloning[32]or Gibson Assembly (NEB) were employed for plasmid
583 assembly. Briefly, PCR was performed with Q5 polymerase (NEB) to generate cloning inserts. In
584 the case of pTOX2[33], linear plasmid backbone was generated by restriction digestion with SwaI
585 (NEB). Inserts in assembled plasmids were verified by sequencing (Azenta Genewiz or
586 Plasmidsuarus). Plasmids used in this study are listed in Table S5. Transfer of plasmids into
587 *V. parahaemolyticus* was accomplished by conjugation with *E. coli* S17 or MFD*pir*[34] (a DAP
588 auxotroph) followed by selective plating on LB plates containing appropriate antibiotics. Mutants
589 were generated by allelic exchange with 15% sucrose (pRE112 backbone) or 2% rhamnose (pTOX2
590 backbone) for counter selection. Mutations were verified by colony PCR or Sanger sequencing. To
591 insert antibiotic cassettes into the phage VP882 genome, PCR products containing the antibiotic
592 cassette flanked by homologous phage VP882 DNA sequences were introduced by natural
593 transformation. Competence of *V. parahaemolyticus* 882 was induced by expression of *tfoX*[35].
594 Phages carrying antibiotic cassettes were isolated by lysogenization of *V. parahaemolyticus* 882
595 that had previously been cured of phage VP882.
596
597 **Generation of phage lysates**
598 Overnight cultures of *V. parahaemolyticus* 882 strains lysogenized with phage VP882 were diluted
599 1:100 in LM and incubated for 2 h at 30 °C with aeration (180 rpm). Mitomycin C was added and
600 growth continued for 2.5 h. Lysates of lytic phage VP882 were generated by infection of *V.*
601 *parahaemolyticus* 882 that had been cured of phage VP882 for 16 h at 30 °C with aeration. Debris
602 was removed from lysed cultures by centrifugation (10,000 x g for 1 min). Clarified supernatant
603 was treated with 0.5 % chloroform for at least 15 min prior to use. Phage lysate titers were
604 quantified by plaque assay.
605
606 **Phage VP882 plaque assay**

607 Phage VP882 plaquing on *V. parahaemolyticus* strains was quantified by the double-layer overlay
608 plaque method[36]. *V. parahaemolyticus* was grown from a single colony to stationary phase (16 h).
609 The culture was diluted 1:100 into molten 0.5% LB agar containing 10 mM $CaCl_2$. The mixture was
610 poured over 1.5% LB agar in a petri plate and allowed to solidify at room temperature for 10-15
611 min. 0.1% Evan's Blue (Sigma) and 0.2% uranine (Sigma) were incorporated into the bottom agar
612 to enhance plaque visibility. 10-fold serial dilutions of phage VP882 lysate (initial titer 10^{-8}-10^{-9}
613 PFU/mL) were spotted onto the plate (3.5 µL/spot) and allowed to dry prior to incubation
614 overnight at 37 °C. Plaques were imaged with an IQ800 imager (Cytvia) using the UV setting and
615 black tray with 0.1 s exposure. Because phage VP882 does not form individual plaques on *V.*
616 *parahaemolyticus* in high cell density QS mode, plaquing was assessed based on clearance and
617 the sizes of plaques as described previously[37]. The lowest 10-fold dilution spot in which clearance
618 occurred was recorded. The log differences in plaquing shown in Figures 3A and S2A are the
619 differences between the plaquing score for the parent *V. parahaemolyticus* 882 strain cured of
620 phage VP882 and the designated strain.
621
622 **Phage VP882 adsorption assay**
623 *V. parahaemolyticus* was grown from a single colony to stationary phase (16 h). The culture was
624 adjusted to OD_{600} 2.5 with LB. 50 µL of this culture was combined with 150 µL of a suspension
625 containing 10 mM $CaCl_2$ and lysate from a spontaneously occurring lytic phage VP882 variant
626 (final MOI 10^{-3}-10^{-4}). The mixture was incubated at room temperature for 20 min. Cells and
627 adsorbed phage particles were separated from free phage by centrifugation (10,000 x g for 1 min).
628 30 µL of the free phage solution was added to 4 mL of 0.5% LB agar containing 10 mM $CaCl_2$ and
629 a 1:100 dilution of a stationary phase culture of *V. parahaemolyticus* 882 that had been cured of
630 phage VP882. The mixture was poured into 3 cm petri dishes (Falcon). Plaques were quantified
631 after overnight incubation at 37 °C. The fraction of unadsorbed phage (% free phage) was
632 calculated by comparing the number of phage to that in an identically treated sample lacking
633 bacteria.
634
635 **Phage VP882 lysogenization assay**
636 *V. parahaemolyticus* was grown from a single colony to stationary phase (16 h). The culture was
637 adjusted to OD_{600} 2.5 with LB. The cell suspension was mixed at a 1:4 ratio with a suspension
638 containing LB, 10 mM $CaCl_2$, and lysate from phage VP882 marked with an antibiotic cassette at
639 an MOI 10^{-5}-10^{-6}. The mixture was incubated without shaking at 30 °C for 1 h prior to plating on
640 nonselective medium to quantify total cells and on selective medium to quantify lysogens. For
641 experiments to test lysogenization of *V. parahaemolyticus* lacking the O3:K6 K-antigen receptor,
642 the entire lysogenization mixture was diluted into 3 mL of fresh LM containing 10 mM $CaCl_2$ and
643 grown for 16 h at 30 °C with aeration before plating on selective medium. Plates were incubated
644 at 37 °C for 16-20 h and colonies counted. Percent lysogens is the number of colonies on selective
645 medium divided by the number on nonselective medium. In all lysogenization quantitation
646 experiments except those examining phage recombination, phage VP882$^{gp38::\mathrm{Cm}}$ was used. In
647 experiments examining phage recombination, lysogens harboring phage VP882$^{gp71\text{-intergenic::Cm}}$
648 were infected with phage VP882$^{gp38::\mathrm{Gm}}$ lysate. Lysogens resistant to both gentamicin and
649 chloramphenicol were isolated and purified to verify dual-resistance. Homogeneity of each locus
650 was assessed by colony PCR with DreamTaq Polymerase (Thermo). PCR products were analyzed

651 on 1% agarose 1X TAE gels stained with SYBR Safe (Edvotek) and imaged with an IQ800 imager
652 (Cytvia) using the Cy2 setting and black tray with auto-exposure.
653
654 **Construction of transposon mutant libraries**
655 Transposon insertion libraries in *V. parahaemolyticus* 882 or *V. parahaemolyticus* 882 *luxO*^{D61A}
656 both of which had been cured of phage VP882 were generated with the Mariner transposon on
657 pSC189 using kanamycin selection[38]. *E. coli* MFD*pir*/pSC189 was used as the donor to deliver
658 pSC189 by conjugation. 300 µL of donor and 100 µL of recipient were mixed. The suspension was
659 subjected to centrifugation (8,000 x g for 2 min) and 390 µL of the clarified culture fluid was
660 removed. Cells were resuspended in the residual medium and spotted on 0.45 µm mixed cellulose
661 ester membrane filters (Millipore) that had been placed onto LB agar plates followed by
662 incubation at 37 °C for 2 h. The filters were transferred to microcentrifuge tubes containing 1 mL
663 of PBS and subjected to vortex to dislodge cells. Various dilutions of the cell suspensions were
664 plated on nonselective and selective media to quantify the number of exconjugants. 10 separate
665 matings were performed to generate the library. Each mating yielded ~35,000-70,000
666 exconjugants. Nested arbitrary PCR (Neo-F + Arb 1, pSC189-1st-3rd + Arb2)[39] was used to assess
667 randomness of transposition. Exconjugants were collected from the plates by scraping all colonies
668 into LB broth containing appropriate antibiotics, resulting in cell suspensions of OD_{600} of ~50.
669 Aliquots of the library were frozen in 30% glycerol.
670
671 **Transposon mutagenesis screen to identify genes encoding the phage VP882 receptor**
672 pBAD-*q* was introduced into the phage-cured *V. parahaemolyticus* 882 transposon mutants from
673 the above library by conjugation. Exconjugants were selected on LB agar containing
674 chloramphenicol and kanamycin. Selection of survivors of phage VP882 infection was performed
675 by diluting the library of mutants containing pBAD-*q* 1:2,000 or 1:20,000 into 8 separate 10 mL
676 aliquots of LB containing 10 mM $CaCl_2$ and phage VP882 to yield 8 different ratios of phage:
677 bacteria at MOI 0.001-2 followed by incubation for 16 h. The infected cultures were back-diluted
678 1:150 into LB broth and grown for 2.5 h at 30 °C with aeration. Subsequently, 0.2% arabinose was
679 added to induce expression of *q* and the cultures grown for 2 h at 30 °C with aeration before
680 plating. Colonies were screened for phage VP882 by PCR for $vqmA_{Phage}$ (primers oMRS1 + oMRS2).
681 All opaque colonies were positive for phage VP882 indicating that they were lysogens (see main
682 text). Phage-free colonies were isolated, and the transposon insertion sites were identified by
683 arbitrary PCR and Sanger sequencing with the pSC189-1st-3rd primer.
684
685 **Transposon mutagenesis screen to identify genes encoding factors that prevent phage VP882**
686 **infection of *V. parahaemolyticus* 882 at high cell density**
687 A thawed aliquot of the *V. parahaemolyticus* 882 *luxO*^{D61A} transposon mutant library was diluted
688 1:1,000 in 20 mL of LB broth and incubated for 30 min at 30 °C with aeration for resuscitation.
689 The suspension was diluted into 10 tubes containing 10 mM $CaCl_2$ and phage VP882$^{gp38::Cm}$ at MOI
690 10^{-5}-10^{-6}, incubated for 3 h with aeration and then plated on LB + chloramphenicol + kanamycin
691 to select lysogens. Plates were incubated for 20 h at 37 °C and then at room temperature for an
692 additional 24 h. Chloramphenicol-resistant colonies were isolated and transposon insertion sites
693 were identified by arbitrary PCR and Sanger sequencing with the pSC189-1st-3rd primer.
694

695 **Quantitation and statistical analyses**
696 Software used to collect and analyze data generated in this study consisted of: GraphPad Prism
697 10 for visualization of data, calculation of statistics, and analysis of growth and reporter-based
698 experiments; Gen5 for collection of growth and reporter-based data; Geneious v2026.0 for
699 primer design and sequencing verification; Amersham ImageQuant for imaging of plaque assays
700 and agarose gels. Data are presented as the means ± SEMs. Numbers of technical and
701 independent biological replicates are indicated in the figure legends.

References

1. Howard-Varona, C., Hargreaves, K.R., Abedon, S.T., and Sullivan, M.B. (2017). Lysogeny in nature: mechanisms, impact and ecology of temperate phages. ISME J. *11*, 1511–1520. https://doi.org/10.1038/ismej.2017.16.
2. Cheong, K.H., Wen, T., Benler, S., Koh, J.M., and Koonin, E.V. (2022). Alternating lysis and lysogeny is a winning strategy in bacteriophages due to Parrondo's paradox. Proc. Natl. Acad. Sci. *119*, e2115145119. https://doi.org/10.1073/pnas.2115145119.
3. Erez, Z., Steinberger-Levy, I., Shamir, M., Doron, S., Stokar-Avihail, A., Peleg, Y., Melamed, S., Leavitt, A., Savidor, A., Albeck, S., et al. (2017). Communication between viruses guides lysis–lysogeny decisions. Nature *541*, 488–493. https://doi.org/10.1038/nature21049.
4. Li, G., Cortez, M.H., Dushoff, J., and Weitz, J.S. (2020). When to be temperate: on the fitness benefits of lysis vs. lysogeny. Virus Evol. *6*, veaa042. https://doi.org/10.1093/ve/veaa042.
5. Papenfort, K., and Bassler, B.L. (2016). Quorum sensing signal-response systems in Gram-negative bacteria. Nat. Rev. Microbiol. *14*, 576–588. https://doi.org/10.1038/nrmicro.2016.89.
6. Silpe, J.E., and Bassler, B.L. (2019). A host-produced quorum-sensing autoinducer controls a phage lysis-lysogeny decision. Cell *176*, 268-280.e13. https://doi.org/10.1016/j.cell.2018.10.059.
7. Silpe, J.E., Duddy, O.P., and Bassler, B.L. (2022). Natural and synthetic inhibitors of a phage-encoded quorum-sensing receptor affect phage–host dynamics in mixed bacterial communities. Proc. Natl. Acad. Sci. *119*, e2217813119. https://doi.org/10.1073/pnas.2217813119.
8. Kaiser, A.D., and Jacob, F. (1957). Recombination between related temperate bacteriophages and the genetic control of immunity and prophage localization. Virology *4*, 509–521. https://doi.org/10.1016/0042-6822(57)90083-1.
9. Brown, S., Mitarai, N., and Sneppen, K. (2022). Protection of bacteriophage-sensitive Escherichia coli by lysogens. Proc. Natl. Acad. Sci. U. S. A. *119*, e2106005119. https://doi.org/10.1073/pnas.2106005119.
10. Łoś, J., Zielińska, S., Krajewska, A., Michalina, Z., Małachowska, A., Kwaśnicka, K., and Łoś, M. (2021). Temperate Phages, Prophages, and Lysogeny. In Bacteriophages, D. R. Harper, S. T. Abedon, B. H. Burrowes, and M. L. McConville, eds. (Springer International Publishing), pp. 119–150. https://doi.org/10.1007/978-3-319-41986-2_3.
11. Bondy-Denomy, J., Qian, J., Westra, E.R., Buckling, A., Guttman, D.S., Davidson, A.R., and Maxwell, K.L. (2016). Prophages mediate defense against phage infection through diverse mechanisms. ISME J. *10*, 2854–2866. https://doi.org/10.1038/ismej.2016.79.
12. Bucher, M.J., and Czyż, D.M. (2024). Phage against the machine: the SIE-ence of superinfection exclusion. Viruses *16*, 1348. https://doi.org/10.3390/v16091348.
13. Wright, A. (1971). Mechanism of conversion of the *Salmonella* O antigen by bacteriophage ε^{34}. J. Bacteriol. *105*, 927–936. https://doi.org/10.1128/jb.105.3.927-936.1971.
14. Uc-Mass, A., Loeza, E.J., De La Garza, M., Guarneros, G., Hernández-Sánchez, J., and Kameyama, L. (2004). An orthologue of the cor gene is involved in the exclusion of temperate lambdoid phages. Evidence that Cor inactivates FhuA receptor functions. Virology *329*, 425–433. https://doi.org/10.1016/j.virol.2004.09.005.

15. Broadbent, S.E., Davies, M.R., and Van Der Woude, M.W. (2010). Phase variation controls expression of *Salmonella* lipopolysaccharide modification genes by a DNA methylation-dependent mechanism. Mol. Microbiol. *77*, 337–353. https://doi.org/10.1111/j.1365-2958.2010.07203.x.
16. Leavitt, J.C., Woodbury, B.M., Gilcrease, E.B., Bridges, C.M., Teschke, C.M., and Casjens, S.R. (2024). Bacteriophage P22 SieA-mediated superinfection exclusion. mBio *15*, e02169-23. https://doi.org/10.1128/mbio.02169-23.
17. Taylor, V.L., Patel, P.H., Shah, M., Yusuf, A., Burk, C.M., Sztanko, K.M., Gitai, Z., Davidson, A.R., Koch, M.D., and Maxwell, K.L. (2025). Prophages block cell surface receptors to preserve their viral progeny. Nature *644*, 1049–1057. https://doi.org/10.1038/s41586-025-09260-z.
18. Papenfort, K., Silpe, J.E., Schramma, K.R., Cong, J.-P., Seyedsayamdost, M.R., and Bassler, B.L. (2017). A *Vibrio cholerae* autoinducer-receptor pair that controls biofilm formation. Nat. Chem. Biol. *13*, 551–557. https://doi.org/10.1038/nchembio.2336.
19. Papenfort, K., Förstner, K.U., Cong, J.-P., Sharma, C.M., and Bassler, B.L. (2015). Differential RNA-seq of *Vibrio cholerae* identifies the VqmR small RNA as a regulator of biofilm formation. Proc. Natl. Acad. Sci. *112*. https://doi.org/10.1073/pnas.1500203112.
20. Duddy, O.P., Silpe, J.E., Fei, C., and Bassler, B.L. (2023). Natural silencing of quorum-sensing activity protects *Vibrio parahaemolyticus* from lysis by an autoinducer-detecting phage. PLoS Genet. *19*, e1010809. https://doi.org/10.1371/journal.pgen.1010809.
21. Huang, X., Duddy, O.P., Silpe, J.E., Paczkowski, J.E., Cong, J., Henke, B.R., and Bassler, B.L. (2020). Mechanism underlying autoinducer recognition in the *Vibrio cholerae* DPO-VqmA quorum-sensing pathway. J. Biol. Chem. *295*, 2916–2931. https://doi.org/10.1074/jbc.RA119.012104.
22. Silpe, J.E., Bridges, A.A., Huang, X., Coronado, D.R., Duddy, O.P., and Bassler, B.L. (2020). Separating functions of the phage-encoded quorum-sensing-activated antirepressor Qtip. Cell Host Microbe *27*, 629-641.e4. https://doi.org/10.1016/j.chom.2020.01.024.
23. Santoriello, F.J., and Bassler, B.L. (2024). The LuxO-OpaR quorum-sensing cascade differentially controls Vibriophage VP882 lysis-lysogeny decision making in liquid and on surfaces. PLOS Genet. *20*, e1011243. https://doi.org/10.1371/journal.pgen.1011243.
24. Chen, Y., Dai, J., Morris, J.G., and Johnson, J.A. (2010). Genetic analysis of the capsule polysaccharide (K antigen) and exopolysaccharide genes in pandemic Vibrio parahaemolyticus O3:K6. BMC Microbiol. *10*, 274. https://doi.org/10.1186/1471-2180-10-274.
25. Santoriello, F.J., and Bassler, B.L. (2026). A family of linear plasmid phages that detect a quorum-sensing autoinducer exists in multiple bacterial species. mBio *17*, e02320-25. https://doi.org/10.1128/mbio.02320-25.
26. Whitfield, C. (2009). Structure and assembly of *Escherichia coli* capsules. EcoSal Plus *3*, 10.1128/ecosalplus.4.7.3. https://doi.org/10.1128/ecosalplus.4.7.3.
27. Shao, Y., Feng, L., Rutherford, S.T., Papenfort, K., and Bassler, B.L. (2013). Functional determinants of the quorum-sensing non-coding RNAs and their roles in target regulation. EMBO J. *32*, 2158–2171. https://doi.org/10.1038/emboj.2013.155.
28. Høyland-Kroghsbo, N.M., Mærkedahl, R.B., and Svenningsen, S.L. (2013). A quorum-sensing-induced bacteriophage defense mechanism. mBio *4*, e00362-12. https://doi.org/10.1128/mBio.00362-12.

29. Tan, D., Svenningsen, S.L., and Middelboe, M. (2015). Quorum sensing determines the choice of antiphage defense strategy in vibrio anguillarum. mBio *6*, e00627. https://doi.org/10.1128/mBio.00627-15.
30. Patterson, A.G., Jackson, S.A., Taylor, C., Evans, G.B., Salmond, G.P.C., Przybilski, R., Staals, R.H.J., and Fineran, P.C. (2016). Quorum sensing controls adaptive immunity through the regulation of multiple CRISPR-Cas systems. Mol. Cell *64*, 1102–1108. https://doi.org/10.1016/j.molcel.2016.11.012.
31. Høyland-Kroghsbo, N.M., Paczkowski, J., Mukherjee, S., Broniewski, J., Westra, E., Bondy-Denomy, J., and Bassler, B.L. (2017). Quorum sensing controls the *Pseudomonas aeruginosa* CRISPR-Cas adaptive immune system. Proc. Natl. Acad. Sci. *114*, 131–135. https://doi.org/10.1073/pnas.1617415113.
32. Li, C., Wen, A., Shen, B., Lu, J., Huang, Y., and Chang, Y. (2011). FastCloning: a highly simplified, purification-free, sequence- and ligation-independent PCR cloning method. BMC Biotechnol. *11*, 92. https://doi.org/10.1186/1472-6750-11-92.
33. Lazarus, J.E., Warr, A.R., Kuehl, C.J., Giorgio, R.T., Davis, B.M., and Waldor, M.K. (2019). A new suite of allelic-exchange vectors for the scarless modification of proteobacterial genomes. Appl. Environ. Microbiol. *85*, e00990-19. https://doi.org/10.1128/AEM.00990-19.
34. Ferrières, L., Hémery, G., Nham, T., Guérout, A.-M., Mazel, D., Beloin, C., and Ghigo, J.-M. (2010). Silent mischief: Bacteriophage Mu insertions contaminate products of <Escherichia coli</i> random mutagenesis performed using suicidal transposon delivery plasmids mobilized by broad-host-range RP4 conjugative machinery. J. Bacteriol. *192*, 6418–6427. https://doi.org/10.1128/JB.00621-10.
35. Chimalapati, S., De Souza Santos, M., Servage, K., De Nisco, N.J., Dalia, A.B., and Orth, K. (2018). Natural Transformation in *Vibrio parahaemolyticus* : a Rapid Method To Create Genetic Deletions. J. Bacteriol. *200*. https://doi.org/10.1128/JB.00032-18.
36. Hershey, A.D., Kalmanson, G., and Bronfenbrenner, J. (1943). Quantitative methods in the study of the phage-antiphage reaction. J. Immunol. *46*, 267–279. https://doi.org/10.4049/jimmunol.46.5.267.
37. Sargen, M.R., Antine, S.P., Grabe, G.J., Antonellis, G., Ragucci, A.E., Li, Y., Kranzusch, P.J., and Helaine, S. (2026). A prophage-encoded abortive infection protein preserves host and prophage spread. Nature. https://doi.org/10.1038/s41586-025-10070-6.
38. Chiang, S.L., and Rubin, E.J. (2002). Construction of a mariner -based transposon for epitope-tagging and genomic targeting. Gene *296*, 179–185. https://doi.org/10.1016/S0378-1119(02)00856-9.
39. Truong, T.T., Vettiger, A., and Bernhardt, T.G. (2020). Cell division is antagonized by the activity of peptidoglycan endopeptidases that promote cell elongation. Mol. Microbiol. *114*, 966–978. https://doi.org/10.1111/mmi.14587.
40. Lan, S.-F., Huang, C.-H., Chang, C.-H., Liao, W.-C., Lin, I.-H., Jian, W.-N., Wu, Y.-G., Chen, S.-Y., and Wong, H.-C. (2009). Characterization of a new plasmid-like prophage in a pandemic *Vibrio parahaemolyticus* O3:K6 strain. Appl. Environ. Microbiol. *75*, 2659–2667. https://doi.org/10.1128/AEM.02483-08.
41. Makino, K., Oshima, K., Kurokawa, K., Yokoyama, K., Uda, T., Tagomori, K., Iijima, Y., Najima, M., Nakano, M., Yamashita, A., et al. (2003). Genome sequence of *Vibrio parahaemolyticus:*

a pathogenic mechanism distinct from that of *V. cholerae*. The Lancet *361*, 743–749. https://doi.org/10.1016/S0140-6736(03)12659-1.

42. Simon, R., Priefer, U., and Pühler, A. (1983). A broad host range mobilization system for in vivo genetic engineering: Transposon mutagenesis in gram negative bacteria. Bio/Technology *1*, 784–791. https://doi.org/10.1038/nbt1183-784.
43. Sargen, M.R., and Helaine, S. (2024). A prophage competition element protects Salmonella from lysis. Cell Host Microbe *32*, 2063-2079.e8. https://doi.org/10.1016/j.chom.2024.10.012.
44. Lan, S.-F., Huang, C.-H., Chang, C.-H., Liao, W.-C., Lin, I.-H., Jian, W.-N., Wu, Y.-G., Chen, S.-Y., and Wong, H. (2009). Characterization of a new plasmid-like prophage in a pandemic *Vibrio parahaemolyticus* O3:K6 strain. Appl. Environ. Microbiol. *75*, 2659–2667. https://doi.org/10.1128/AEM.02483-08.

Table S1: Transposon insertion sites identified in the screen for the phage VP882 receptor.

Sequence Number	Insertion Site	Direction	Gene ID
1	231439	forward	*VP0220*
2	234489	forward	*VP0221*
3	234489	forward	*VP0221*
4	235609	forward	*VP0222*
5	235779	forward	*VP0222*
6	235855	forward	*VP0222*
7	235855	forward	*VP0222*
8	237039	forward	*VP0224*
9	243061	forward	*VP0230*
10	243498	reverse	*VP0231*
11	243643	forward	*VP0230*
12	243914	forward	*VP0230*
13	244073	forward	*VP0230*
14	244219	forward	*VP0231*
15	244285	forward	*VP0231*
16	244285	forward	*VP0231*
17	244479	forward	*VP0231*
18	249145	forward	*VP0235*
19	249360	reverse	*VP0235*

Table S2: Transposon insertion sites identified in the screen for the factor that prevents phage VP882 adsorption to *V. parahaemolyticus.*

Insertions in *VPA1602-4* are shaded gray

* indicates the read quality was too poor to identify the insertion site

Sequence Number	Insertion Site	Direction	Disrupted locus	Annotation
Chromosome 1				
1	77696	reverse	*VP0068*	*gorA*
2	92662	reverse	*VP0081*	BON Domain protein
3	183123	forward	*VP0168-VP0170*, intergenic	TonB-dependent receptor plug domain-containing protein and ABC transporter
4	102615	reverse	*VP0109*	*engB*
5	128809	reverse	*VP0120*	*glnL*
6	196839	reverse	*VP0183*	Methyl accepting chemotaxis protein
7	*	forward	*VP0199*	*neuC*
8	209620	forward	5' *VP0199*	5' of *neuC*
9	210461	forward	*VP0199*	*neuC*
10	253049	reverse	*VP0238*	MBL fold metallo-hydrolase
11	379167	forward,	5' *VP0377*	HTH domain protein
12	390779	forward	3' *VP0388*	methylase
13	426994	forward	*VP0424*	*hldE*
14	508389	forward	*VP0494*	*thrA*
15	545647	reverse	*VP0527*	*nhaR*
16	630725	forward	*VP0605*	rRNA large subunit methyltransferase N
17	681151	reverse	*VP06050, VP06051* intergenic	*nadK, grpE*
18	*	forward	*VP0682*	*ribH*
19	716483	forward	*VP0684*	*thiL*
20	827688	forward	5' *VP0793*	*crr*
21	*	reverse	*VP0831*	*nagE*
22	1022658	reverse	*VP0980*	DUF2062 domain protein
23	*	forward	*VP1231*	*fabV*
24	1386862	reverse	*VP1305/VP1306*	*cobU,* adenosylcobinamide-GDP ribazoletransferase
25	1421362	reverse	*VP1340*	Collagenase
26	2292011	reverse	3' *VP2183*	Response regulator

27	2549724	forward	*VP2429-VP2430,* intergenic	*radA*
28	2643101	forward	*VP2504*	*pcnB*
29	2688526	forward	5' *VP2546*	*csrA*
30	2688526	forward	5' *VP2546*	*csrA*
31	2723599	forward	*VP2577*	*rseA*
32	2723599	forward	*VP2577*	*rseA*
33	2755274	reverse	*VP2611*	*gshB*
34	2833881	forward	*VP2683*	PhoH family protein
35	2867011	forward	*VP2711*	*galU*
36	2971496	reverse	*VP2807*	*rnr*
37	3055472	forward	*VP2884*	*dusB*
38	3056590	forward	*VP2885*	*fis*
39	3056590	forward	*VP2885*	*fis*
40	3070488	reverse	*VPr018*	23S rRNA
41	3100523	forward	*VP2911*	5' of *hupA*
42	3220203	reverse	*VP3016*	HvfC/BufC N-terminal domain-containing protein
43	3247914	forward	*VP3041*	LysM domain protein
Chromosome 2				
44	37139	forward	*VPA0045*	Ada regulatory protein
45	44076	reverse	*VPA0063*	Hypothetical protein
46	452925	reverse	*VPA0495*	AraC family transcriptional regulator
47	*	forward	*VPA0627*	5' of *cyoA*
48	*	forward	*VPA1442*	DUF11 domain protein
48	1560611	forward	*VPA1464*	Lcl domain protein
49	1700868	forward	*VPA1602*	Polysaccharide export protein Wza
50	1700867	forward	*VPA1602*	Polysaccharide export protein Wza
51	1701292	reverse	*VPA1602*	Polysaccharide export protein Wza
52	1700403	forward	5' *VPA1602*	5' of *VPA1602* Polysaccharide export protein Wza
53	1799976	forward	*VPA1678*	*araC*
54	2932536	reverse	*VPA2764*	Homoserine dehydrogenase

Table S3: Strains used in this study

Identifier	Genotype	Plasmid/Phage	Source
V. parahaemolyticus 882			
MRS19		cured	This study, courtesy of O. Duddy
MRS21		VP882$^{gp71\text{-intergenic::Cm}}$	Duddy et al. 2023[20]
MRS34		VP882$^{ctr::Tn5}$	Silpe and Bassler 2019[6]
MRS70		VP882 (native)	Lan et al. 2009[40]
MRS138		Cured; pMRS7	This study
MRS187	*vqmR*$^{+}$-P *vqmA*$_{882}$- *vqmA*$_{882}$:: *vqmA*$_{882}$ (*vqmR-vqmA*882^{+})	cured	This study
MRS188	*luxO*882::*luxO*RIMD (*luxO*$^{+}$)	cured	This study
MRS189	*vqmR*$^{+}$-P*vqmA*$_{882}$- *vqmA*$_{882}$:: *vqmA*$_{882}$; *luxO*882::*luxO*$_{RIMD}$ (*vqmR-vqmA*882^{+} *luxO*$^{+}$)	cured	This study
MRS312	*luxO*$_{882}$::*luxO*^{D61E} (*luxO*^{D61E})	cured	This study
MRS313	*vqmR*$^{+}$-P*vqmA*$_{882}$-*vqmA*$_{882}$::*vqmA*$_{882}$; *luxO*$_{882:}$:*luxO*^{D61E} (*vqmR-vqmA*$_{882}$$^{+}$ *luxO*^{D61E})	cured	This study
MRS314	*luxO*$_{882}$::*luxO*^{D61A} (*luxO*^{D61A})	cured	This study
MRS417	*vqmR*$^{+}$-P*vqmA*$_{882}$-*vqmA*$_{882}$::*vqmA*$_{882}$; *luxO*$_{882:}$:*luxO*^{D61A} (*vqmR-vqmA*$_{882}$$^{+}$ *luxO*^{D61A})	cured	This study
MRS541		VP882 $^{gp38::Cm}$	This study
MRS542		VP882 $^{gp38::Gm}$	This study
MRS550	Δ*VPA1602-1604*	cured	This study
MRS551	*luxO*$_{882}$::*luxO*^{D61A} (*luxO*^{D61A}) Δ*galU*	cured	This study
MRS552	*luxO*$_{882}$::*luxO*^{D61A} (*luxO*^{D61A}) Δ*nagE*	cured	This study
MRS553	*luxO*$_{882}$::*luxO*^{D61A} (*luxO*^{D61A}) Δ*neuC*	cured	This study
MRS554	*luxO*$_{882}$::*luxO*^{D61A} (*luxO*^{D61A}) Δ*VPA1602-1604*	cured	This study
MRS566	*vqmR*$^{+}$-P *vqmA*$_{882}$-*vqmA*882:: *vqmA*$_{882}$ (*vqmR- vqmA*$_{882}$$^{+}$) Δ*VPA1602-1604*	cured	This study
MRS567	*luxO*882::*luxO*$_{RIMD}$ (*luxO*$^{+}$) Δ*VPA1602-1604*	cured	This study
MRS568	*luxO*$_{882}$::*luxO*^{D61E} (*luxO*^{D61E}) Δ*VPA1602-1604*	cured	This study
MRS569	*vqmR*$^{+}$-P*vqmA*$_{882}$-*vqmA*$_{882}$::*vqmA*$_{882}$; *luxO*$_{882:}$:*luxO*^{D61E} (*vqmR-vqmA*$_{882}$$^{+}$ *luxO*^{D61E}) Δ*VPA1602-1604*	cured	This study
MRS571	*vqmR*$^{+}$-P*vqmA*$_{882}$-*vqmA*$_{882}$::*vqmA*$_{882}$; *luxO*$_{882:}$:*luxO*^{D61A} (*vqmR-vqmA*$_{882}$$^{+}$ *luxO*^{D61A}) Δ*VPA1602-1604*		This study
MRS574	*vqmR*$^{+}$-P*vqmA*$_{882}$-*vqmA*$_{882}$::*vqmA*$_{882}$; *luxO*882::*luxO*$_{RIMD}$ (*vqmR- vqmA*$_{882}$$^{+}$ *luxO*$^{+}$) Δ*VPA1602-1604*		
MRS703	Δ*VPA1602-1604*	VP882 (native)	This study
MRS707	*luxO*$_{882}$::*luxO*^{D61A} (*luxO*^{D61A}) Δ*VPA1602-1604*	VP882 (native)	This study
MRS759	Δ*VP0230*	cured	This study
MRS769		VP882 (native); FJS-P073	This study
MRS770	*luxO*882::*luxO*$_{RIMD}$ (*luxO*$^{+}$)	VP882 (native); FJS-P073	This study
MRS806		cured; pMRS70	This study

MRS812	*luxO*$_{882}$::*luxO*^{D61A} (*luxO*^{D61A})	cured; pMRS70	This study
MRS956	*luxO*$_{882}$::*luxO*^{D61A} (*luxO*^{D61A}) Δ*VP0235*		This study
MRS958	Δ*VPA1602-4 ΔVP0235*		This study
MRS959	*luxO*$_{882}$::*luxO*^{D61A} (*luxO*^{D61A}) Δ*VPA1602-1604* Δ*VP0235*		This study
MRS970	Δ*recA*	cured	This study
MRS976	Δ*recA*	VP882 (native)	This study
MRS1011	Δ*recA*	VP882$^{gp71\text{-intergenic::Cm}}$	This study
V. parahaemolyticus VP81			
MRS729	col1		ATCC
MRS730	col2		ATCC
MRS758	col2 *VP0235*$^{+}$		This study
V. parahaemolyticus VP47			
MRS743			ATCC
MRS777	*luxO*$^{+}$		This study
MRS775		FJS-P073	This study
MRS778	*luxO*$^{+}$	FJS-P073	This study
Other *V. parahaemolyticus*			
MRS8	*V. parahaemolyticus* RIMD2210633		Makino et al.[41]
MRS733	*V. parahaemolyticus* VP232		ATCC
MRS734	*V. parahaemolyticus* EB101		ATCC
MRS735	*V. parahaemolyticus* 954		ATCC
MRS736	*V. parahaemolyticus* 205		ATCC
MRS737	*V. parahaemolyticus* 03/4 K30		ATCC
MRS738	*V. parahaemolyticus* 117		ATCC
MRS739	*V. parahaemolyticus* 115		ATCC
MRS740	*V. parahaemolyticus* MDL 3875-7-83		ATCC
MRS741	*V. parahaemolyticus* 10884		ATCC
MRS742	*V. parahaemolyticus* VP250		ATCC
MRS744	*V. parahaemolyticus* FC 1011		ATCC
E. coli strains for cloning and conjugative donors			
E. coli MFDλpir	MG1655 RP4-2-Tc::[ΔMu1::*aac(3)IV*-Δ*aphA*-Δ*nic*35 ΔMu2::*zeo*] Δ*dapA*::(*erm-pir*) Δ*recA*		Ferrières et al. 2010[34]
E. coli S17λ*pir*	Δ*lacU169 (ΦlacZΔM15) recA1 endA1 hsdR17 thi-1 gyrA96 relA1 λpir*		Simon et al. 1983[42]
E. coli TOP10	F- *mcrA* Δ(*mrr-hsdRMS-mcrBC*) Φ80*lacZΔM15* Δ*lacX74 recA1 araD139* Δ(*ara leu*)*7697 galU galK rpsL* (Str^{R}) *endA1 nupG*		Invitrogen
E. coli pir2^{+}	F^{-} Δ*lac*169 *rpo*S(am) *rob*A1 *cre*C510 *hsd*R514 *end*A *rec*A1 *uidA(ΔMlu*I*)*::*pir*		Invitrogen

Table S4: Oligonucleotides used in this study

Identifier	Name	Sequence (5'-3')	Purpose	Source
oMRS1	*qtip*-exR	CCGAAGAAAGCGCAGAAGC	check for presence of phage VP882	This study
oMRS2	VP882-*vqmA*-exR	TGCAATTTGTCGAGAAGGATGC	check for presence of phage VP882	This study
oMRS29	pRE1128-pTOXconvert-F	GTTTAAACCAGGTTAATTAATTTGAGAAGCGGTGTAAGTGAACTG	transfer pRE112 insert to pTOX	This study
oMRS30	pRE1128-pTOXconvert-R	CTCGAGACGTCCCGGGATGCATTTTCTTCTAGAGGTACCGCATGC	transfer pRE112 insert to pTOX	This study
oMRS138	Arb1D	GGCCAGGCCTGCAGATGATGNNNNNNNNNNGTAT	Mariner transposon insertion site identification	Truong et al. 2020[39]
oMRS139	Arb2	GGCCAGGCCTGCAGATGATG	Mariner transposon insertion site identification	Truong et al. 2020[39]
oMRS140	Neo-F	CGTTGGCTACCCGTGATATT	Mariner transposon insertion site identification	Truong et al. 2020[39]
oMRS141	pSC189-1st-3	GGCTGACCGCTTCCTCGTGCTTTAC	Mariner transposon insertion site identification	Truong et al. 2020[39]
oMRS142	*vqmA*host-outer_fwd	ACGCATTTCCTGTACCAGCA	check *vqmRA* of Vpara	This study, courtesy of T.V.P. Nguyen
oMRS143	*vqmA*host-outer_rev	AAGCGATTGGTTTGTTGCGT	check *vqmRA* of Vpara	This study, courtesy of T.V.P. Nguyen
oMRS194	d*VP0235*_downR	TCTTCTAGAGGTACCGCATGCGAATCCAGCTCATTAAAGTATGC	construction of pTOX plasmid for deletion	This study
oMRS195	d*VP0235*_ovF	ATATGGCAACTTGACGCTATACAATTTATGAGTCAATC	construction of pTOX plasmid for deletion	This study
oMRS196	d*VP0235*_ovR	ATAGCGTCAAGTTGCCATATAAATTGTAGACGTTGC	construction of pTOX plasmid for deletion	This study
oMRS197	d*VP0235*_upF	GTAAGTGAACTGCATGAATTCCCGGAATCGATACACGCAGTACTG	construction of pTOX plasmid for deletion	This study
oMRS198	*VP0235*-ex-F	ACGGGAAGTATTGTTGTTAGCTC	check deletion	This study
oMRS199	*VP0235*-ex-R	GACTTCCACAACAAGTAGAATAACC	check deletion	This study
oMRS225	*0230*_downR	CTCGAGACGTCCCGGGATGCATTTACACTACAACTGCCATCATAAGG	construction of pTOX plasmid for deletion	This study
oMRS226	*0230*_upF	GTTTAAACCAGGTTAATTAATTTTTTCTGCATATTCGGTTTGGTTCG	construction of pTOX plasmid for deletion	This study
oMRS231	d*0230*_ovR	TCACCGCCTCAAAGTACTGATGAAGGTATAAAAC	construction of pTOX plasmid for deletion	This study
oMRS232	d*0230*_ovF	TCAGTACTTTGAGGCGGTGAGTGATGAAAAG	construction of pTOX plasmid for deletion	This study
oMRS233	*luxO*vph-ex-F2	GAGGGGTCGCTAATATATCAG	check *luxO* sequence	This study
oMRS27	oMS714	CTGCGCCATCAGATCCTTGG	check insert in pTOX	Sargen and Helaine 2024[43]
oMRS28	oMS715	CGATATCTTCGAACCGGTGC	check insert in pTOX	Sargen and Helaine 2024[43]
oMRS72	*luxO*vph-ex-R	TCAAATACATTAAGCGCTCTGAACC	check genotype	This study
oMRS310	pEVS*lux*_RBS_vectorF	GCTTAACTAAGTAACTAGTACAGG	PCR of pEVS-lux backbone	This study
oMRS311	pEVS*lux*_vector_R	TTAATTAACTCGAGCGGTACC	PCR of pEVS-lux backbone	This study

oMRS409	*gp38*_gm_ovR	GAGAGTAGGGAACTGCCAGGTAGGATCTCCGTTTACCAGTTATAAAT	construction of gentamicin marked *gp38* phage	This study
oMRS410	*gp38*_gm_ovF	ACCCAAGTACCGCCACCTAAAAAAGCCCGCACAAGGCGG	construction of gentamicin marked *gp38* phage	This study
oMRS411	gm_cassette_R	TTAGGTGGCGGTACTTGGGTC	construction of gentamicin marked *gp38* phage	This study
oMRS412	gm_cassette_F	CCTGGCAGTTCCCTACTC	construction of gentamicin marked gp38 phage	This study
oMRS445	*galU*_upF	GTTTAAACCAGGTTAATTAATTTTCTGCAGATTATGTTGTGATTGC	construction of pTOX plasmid for deletion	This study
oMRS446	*galU*_downR	CTCGAGACGTCCCGGGATGCATTTCACTTGGTAAACAATGTTATCTGC	construction of pTOX plasmid for deletion	This study
oMRS447	d*galU*_ovR	GCCTGAACAATTTTAAATTCACCAACTGTAAAAAAGG	construction of pTOX plasmid for deletion	This study
oMRS448	d*galU*_ovF	GAATTTAAAATTGTTCAGGCTCGTTACCAATG	construction of pTOX plasmid for deletion	This study
oMRS449	*nagE*_upF	GTTTAAACCAGGTTAATTAATTTTCAACGCTATGAATACCTTTTTTCG	construction of pTOX plasmid for deletion	This study
oMRS450	*nagE*_downR	CTCGAGACGTCCCGGGATGCATTTGGCTGAACTCGTATTGATGAGG	construction of pTOX plasmid for deletion	This study
oMRS451	d*nagE*_ovR	TTCGATGTAACTTAAGTTCCCCCTATAGGATTC	construction of pTOX plasmid for deletion	This study
oMRS452	d*nagE*_ovF	GGAACTTAAGTTACATCGAACTAATATTTGATTAGAGAC	construction of pTOX plasmid for deletion	This study
oMRS453	*neuC*_upF	GTTTAAACCAGGTTAATTAATTTTACGTAATGGAAACGATTGAGAG	construction of pTOX plasmid for deletion	This study
oMRS454	*neuC*_downR	CTCGAGACGTCCCGGGATGCATTTCCAGAGCCAGGACGTTTAATCG	construction of pTOX plasmid for deletion	This study
oMRS455	d*neuC*_ovR	AATCAGGTTCAACCGCGACCTTTTTCTGTGTC	construction of pTOX plasmid for deletion	This study
oMRS456	d*neuC*_ovF	GGTCGCGGTTGAACCTGATTTAAATAAGAAAGTAGAG	construction of pTOX plasmid for deletion	This study
oMRS457	*VPA16024*_upF	GTTTAAACCAGGTTAATTAATTTGCTCAAAACTGCTTACTGGCAG	construction of pTOX plasmid for deletion	This study
oMRS458	*VPA16024*_downR	CTCGAGACGTCCCGGGATGCATTTATGGCGAAATTATTGCAAGTTGATTTTG	construction of pTOX plasmid for deletion	This study
oMRS459	d*VPA16024*_ovR	CTAGATTAATGTTTTTTCATTCATCTGACGTAAAGAG	construction of pTOX plasmid for deletion	This study
oMRS460	d*VPA16024*_ovF	ATGAAAAAACATTAATCTAGATCGCTAATTTGACC	construction of pTOX plasmid for deletion	This study
oTN0155	P*cat-cat*_fwd	TGATCGGCACGTAAGAGGTTCCAACTTTC	construction of phages marked at *gp38*	This study, courtesy of T.V.P. Nguyen
oTN0156	P*cat-cat*_rev	TTACGCCCCGCCCTGCCA	construction of phages marked at *gp38*	This study, courtesy of T.V.P. Nguyen
oTN0157	upstream-*gp38*_fwd	AGCACGTTGACCAGTCCG	construction of phages marked at *gp38*	This study, courtesy of T.V.P. Nguyen
oTN0158	upstream-*gp38*_rev	ACTGCGATGAGTGGCAGGGCGGGGCGTAATAGGATCTCCGTTTACCAGTTATAAATAATC	construction of phages marked at *gp38*	This study, courtesy of T.V.P. Nguyen
oTN0159	downstream-*gp38*_fwd	GAAAGTTGGAACCTCTTACGTGCCGATCAAAAAGCCCGCACAAGGCG	construction of phages marked at *gp38*	This study, courtesy of T.V.P. Nguyen
oTN0160	downstream-*gp38*_rev	GGACGACTATCGCGGCCA	construction of phages marked at *gp38*	This study, courtesy of T.V.P. Nguyen
oTN0161	delta*gp38*-cmR_fwdcmR_fwd	CGACGAGACGGACATGAGTT	construction of phages marked at *gp38*	This study, courtesy of T.V.P. Nguyen

oTN0169	*gp38*_fwd	GACGGTGAAGGGTAAGGTGG	PCR of *gp38* locus	This study, courtesy of T.V.P.Nguyen
oTN0170	*gp38*_rev	GTCCGTCCTCCTATTTGCCC	PCR of *gp38* locus	This study, courtesy of T.V.P. Nguyen
oMRS598	P*1602*_F3	TTAATACAACGAGATAATTAGTCGG	construction of pMRS70	This study
oMRS599	P*1602*_R2	GCTGGTAGCAACATTCTTCTC	construction of pMRS70	This study
oMRS630	GAB199	AGGTATGGAAGAAGGGACTCG	PCR of *gp71*-intergenic locus	This study, courtesy of G. Beggs
oMRS631	GAB200	CGTCTATTACTTCGCTATCGGATG	PCR of *gp71*-intergenic locus	This study, courtesy of G. Beggs

Table S5: Plasmids used in this study

Identifier	Description	Backbone	Marker	Origin	Construction	Source
pMRS1	pRE112-*VqmA*$_{Vpara}$-ΔFLAG	pRE112	Cm	R6λγpir	Gibson assembly, SmaI site	This study
pMRS3	pTOX2-*VqmA*$_{Vpara}$-ΔFLAG	pTOX2	Cm	R6λγpir	Gibson assembly, SwaI site	This study
pMRS7	pBAD-*q*(CmR)	pEVS	Cm	p15A	Gibson assembly	This study
pMRS12	pTOX2-*VP0235*$^{+}$	pTOX2	Cm	R6λγpir	Gibson assembly, SwaI site	This study
pMRS13	pTOX2-*ΔVP0235*	pTOX2	Cm	R6λγpir	Gibson assembly, SwaI site	This study
pMRS19	pTOX2-Δ*VP0230*	pTOX2	Cm	R6λγpir	Gibson assembly, SwaI site	This study
pMRS22	pTOX2-Δ*recA*	pTOX2	Cm	R6λγpir	FastCloning, SwaI site	This study
pMRS27	pTOX2-Δ*galU*	pTOX2	Cm	R6λγpir	Gibson assembly, SwaI site	This study
pMRS28	pTOX2-Δ*nagE*	pTOX2	Cm	R6λγpir	Gibson assembly, SwaI site	This study
pMRS29	pTOX2-Δ*neuC*	pTOX2	Cm	R6λγpir	Gibson assembly, SwaI site	This study
pMRS30	pTOX2-Δ*VPA1602-1604*	pTOX2	Cm	R6λγpir	Gibson assembly, SwaI site	This study
pMRS70	pEVS-P*VPA1602*(1)-*luxCDABE*	pEVS (Ec1508)	Kan	p15A	FastCloning	This study
FJS-P073	pEVS-P*luxC-luxCDABE*	pEVS	Kan	p15A	X	Santoriello and Bassler 2024[23]
pOD-51	pRE112- *luxO*$_{882}$::*luxO*$_{RIMD}$	pRE112	Cm	R6λγpir	X	Duddy et al. 2023[20]
pSC189	Mariner transposon delivery		Kan/ Amp	R6λγpir	X	Chiang et al. 2002[38]
pMMB-tfoX-sacB	Natural transformation of *V. parahaemolyticus*	pMMB	Kan	pMMB	X	Chimalapati et al. 2018[35]
Plasmid-Phages						
	VP882 (native)	VP882	X	RepA	WT	Lan et al. 2009[44]
MRS-P28	VP882 ^{gp38}::Cm	VP882	Cm	RepA	Natural transformation	This study, courtesy of T.V.P. Nguyen.
MRS-P29	VP882^{gp38}::Gm	VP882	Gm	RepA	Natural transformation	This study
	VP882^{gp71}-intergenic::Cm	VP882	Cm	RepA	Natural transformation	Duddy et al. 2023[20]
	VP882^{ctr}::Tn*5*	VP882	Cm	RepA	Natural transformation	Silpe and Bassler, 2019[6]
MRS-P12	VP882^{gp59}(ΔP98-L120fs)	VP882	X	RepA	Spontaneous frameshift in cI	This study

Graphical Abstract

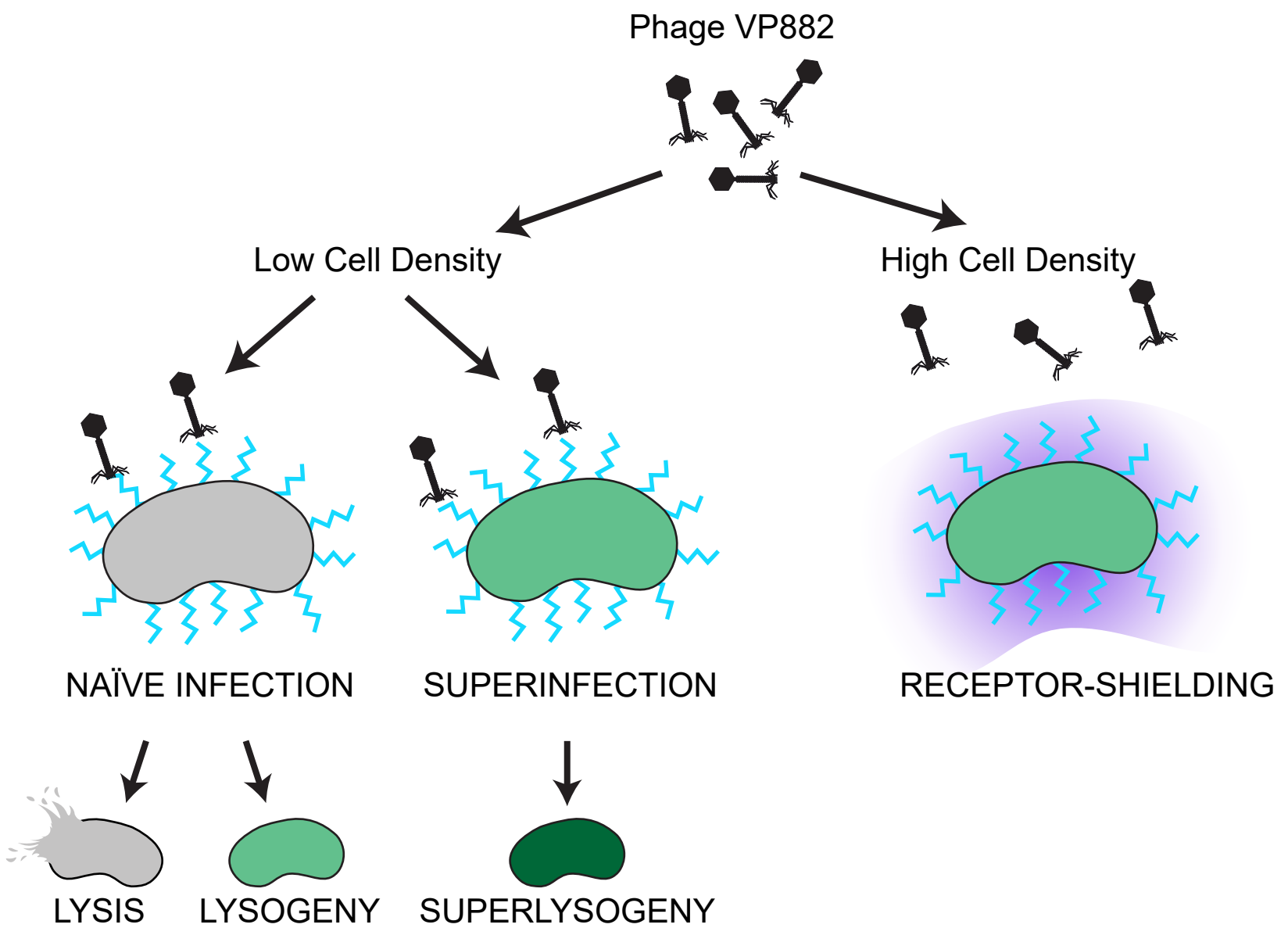

Figure 1

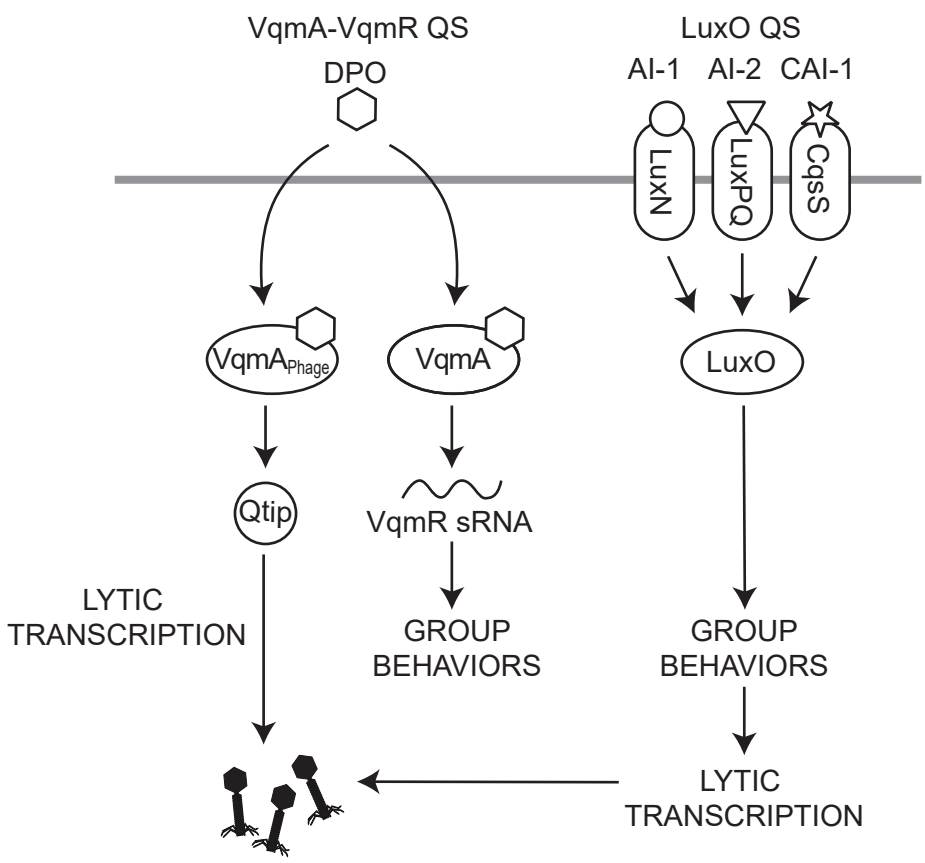
VqmA-VqmR QS
DPO
LuxO QS
AI-1
AI-2
CAI-1
LuxN
LuxPQ
CqsS
VqmA Phage
VqmA
LuxO
Qtip
VqmR sRNA
LYTIC TRANSCRIPTION
GROUP BEHAVIORS
GROUP BEHAVIORS
LYTIC TRANSCRIPTION

Figure 2

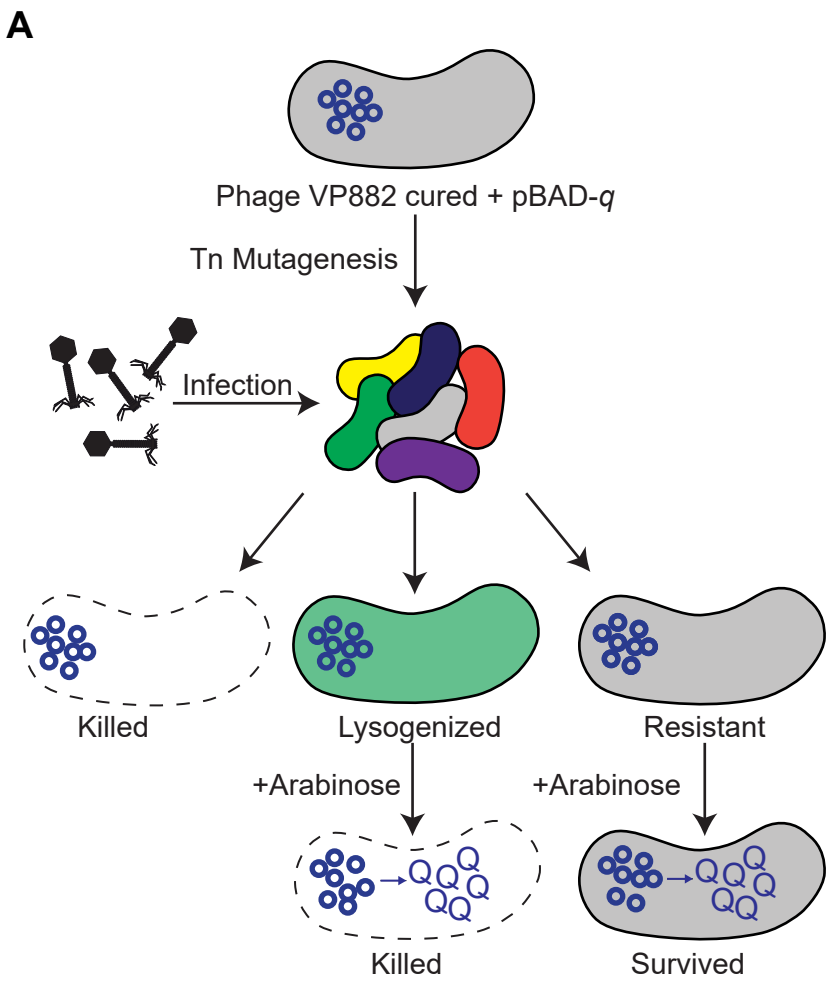

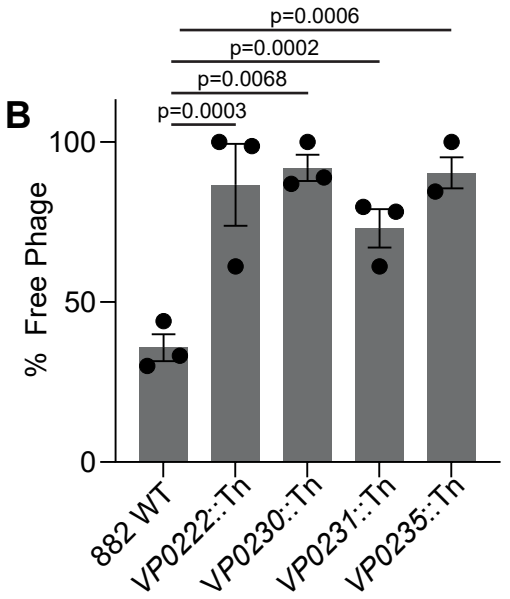

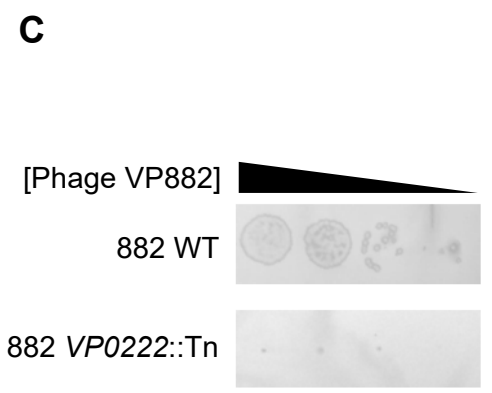

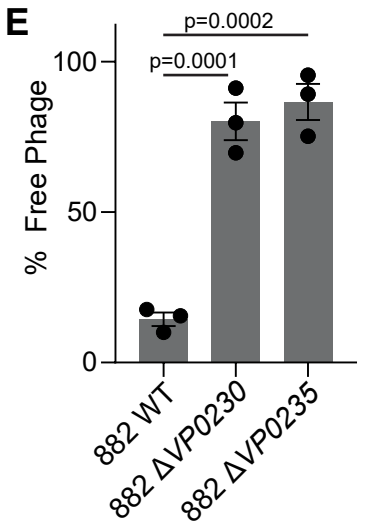

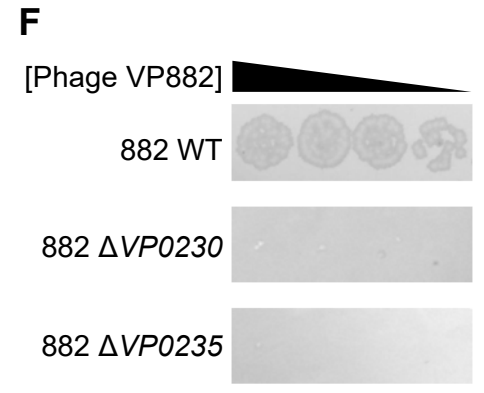

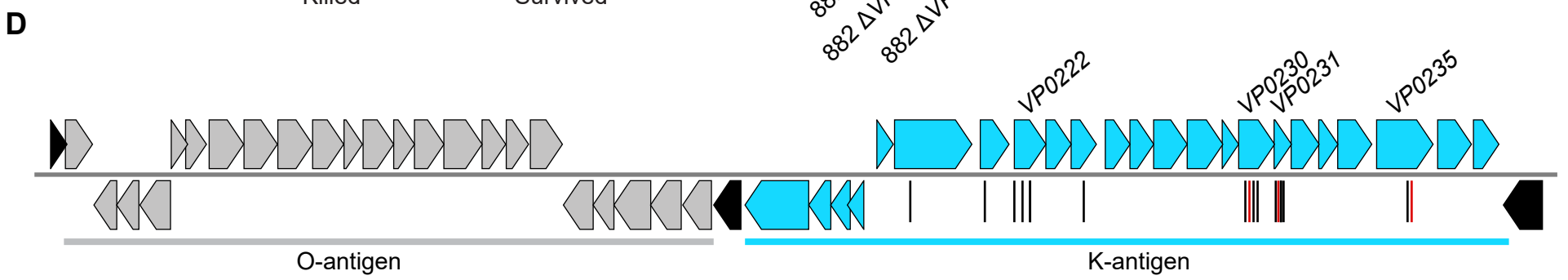

G

Strain	Serotype	Plaquing
882	O3:K6	+
RIMD	O3:K6	+
VP81-col1	O3:K6	+
VP81-col2	O3:K6	-
VP47	O3:K6	+
VP232	O4:K68	-
EB101	undetermined	-
954	not specified	-
205 [9302]	not specified	-
03/4 K30	not specified	-
117 [CDC KC830]	not specified	-
115 [CDC KC824]	not specified	-
MDL 3875-7-83	O4:K12	-
NCTC10884	not specified	-
VP250	O1:KUT	-
FC 1011	not specified	-

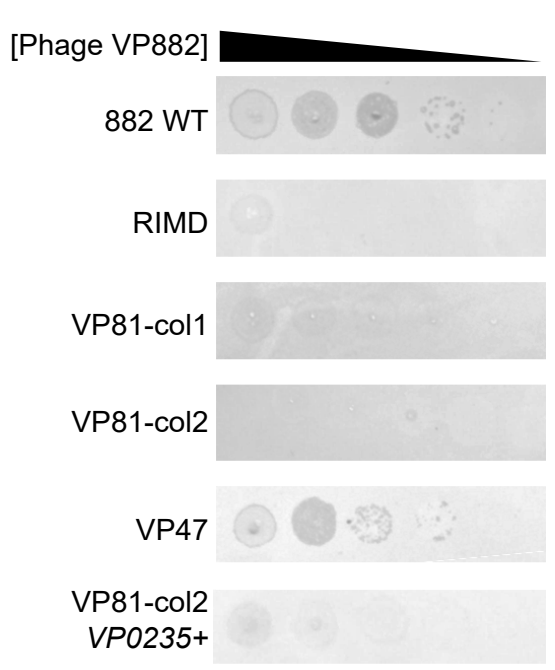

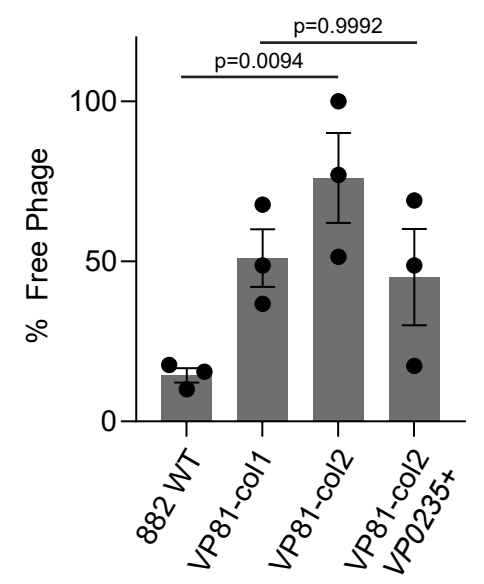

Figure 3

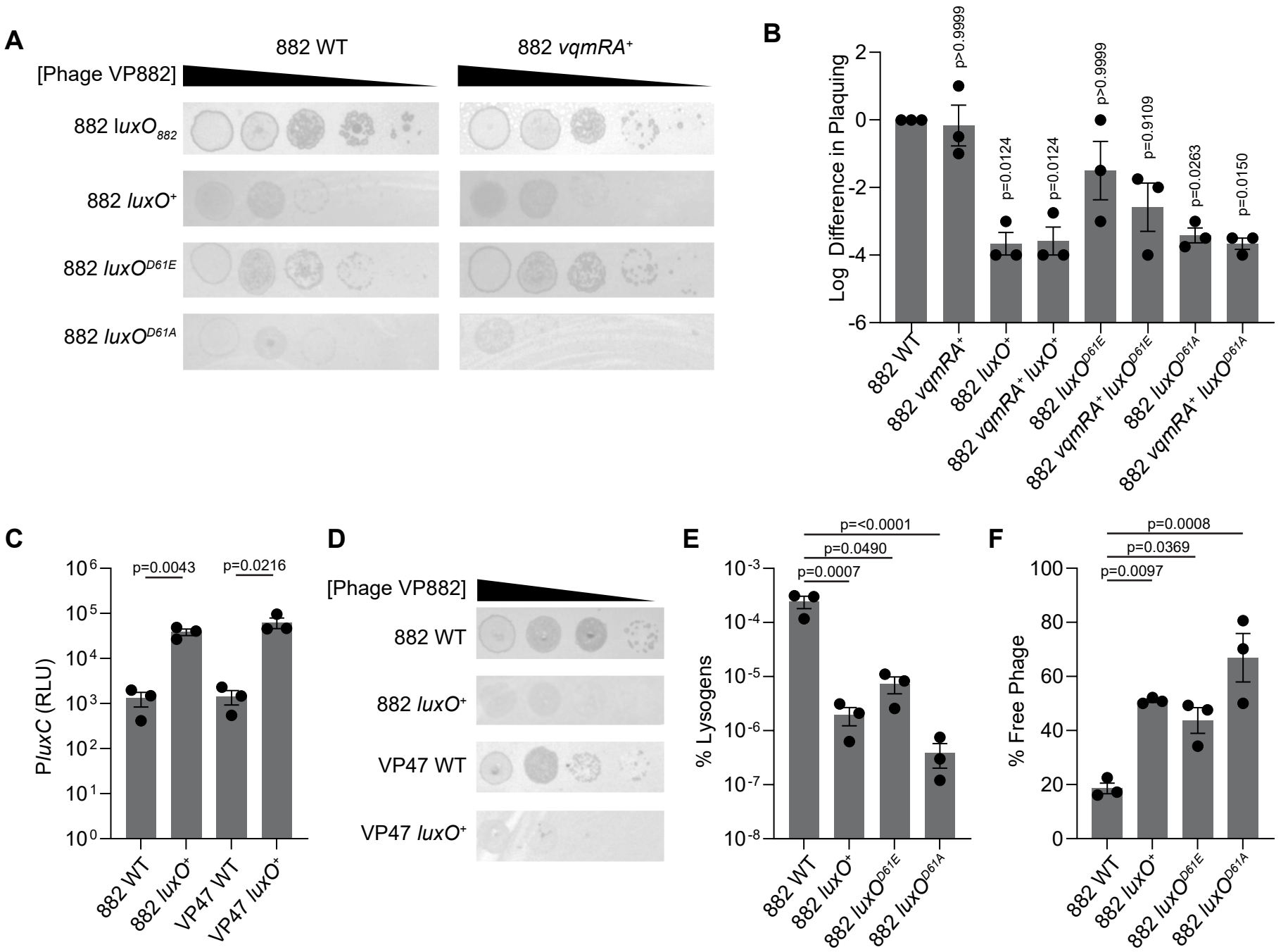
A
882 WT
882 vqmRA+
[Phage VP882]
882 luxO882
882 luxO+
882 luxOD61E
882 luxOD61A
B
Log Difference in Plaquing
p>0.9999
p=0.0124
p=0.0124
p>0.9999
p=0.9109
p=0.0263
p=0.0150
882 WT
882 vqmRA+
882 luxO+
882 vqmRA+ luxO+
882 luxOD61E
882 vqmRA+ luxOD61E
882 luxOD61A
882 vqmRA+ luxOD61A
C
PluxC (RLU)
p=0.0043
p=0.0216
882 WT
882 luxO+
VP47 WT
VP47 luxO+
D
[Phage VP882]
882 WT
882 luxO+
VP47 WT
VP47 luxO+
E
% Lysogens
p=<0.0001
p=0.0490
p=0.0007
882 WT
882 luxO+
882 luxOD61E
882 luxOD61A
F
% Free Phage
p=0.0008
p=0.0369
p=0.0097
882 WT
882 luxO+
882 luxOD61E
882 luxOD61A

Figure 4

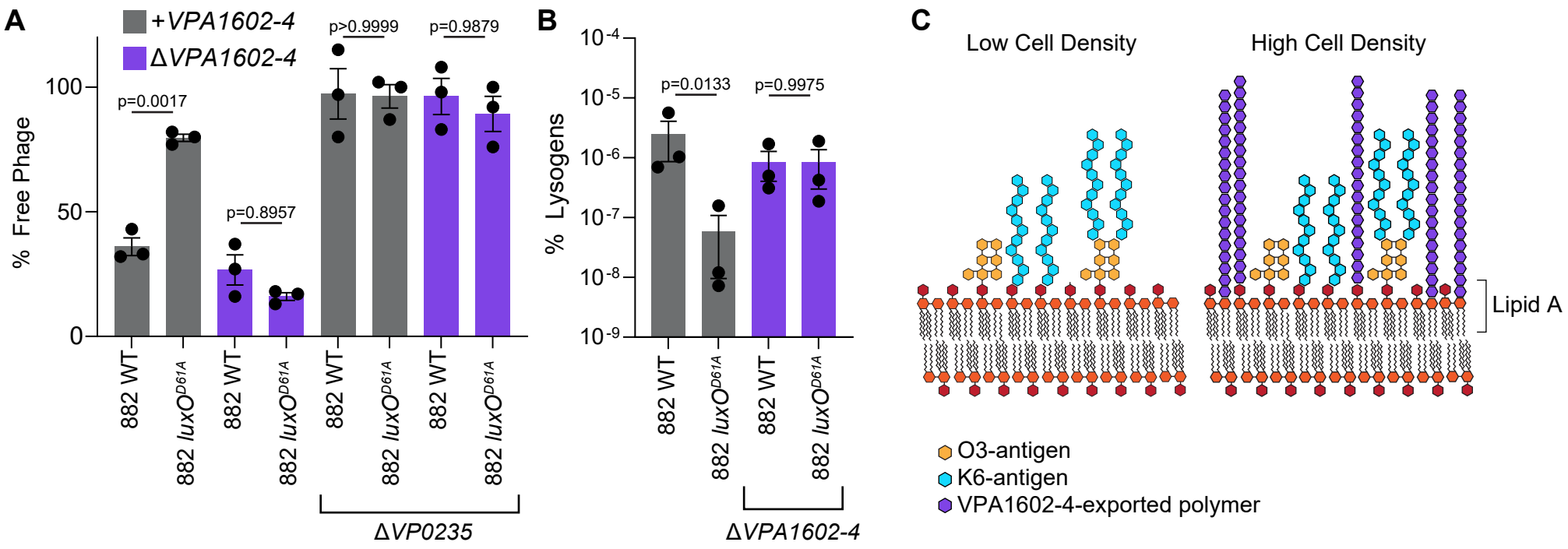
A
+VPA1602-4
ΔVPA1602-4
% Free Phage
100
50
0
p=0.0017
p=0.8957
p>0.9999
p=0.9879
882 WT
882 luxO^D61A
882 WT
882 luxO^D61A
882 WT
882 luxO^D61A
882 WT
882 luxO^D61A
ΔVP0235
B
% Lysogens
10^-4
10^-5
10^-6
10^-7
10^-8
10^-9
p=0.0133
p=0.9975
882 WT
882 luxO^D61A
882 WT
882 luxO^D61A
ΔVPA1602-4
C
Low Cell Density
High Cell Density
Lipid A
O3-antigen
K6-antigen
VPA1602-4-exported polymer

Figure 5

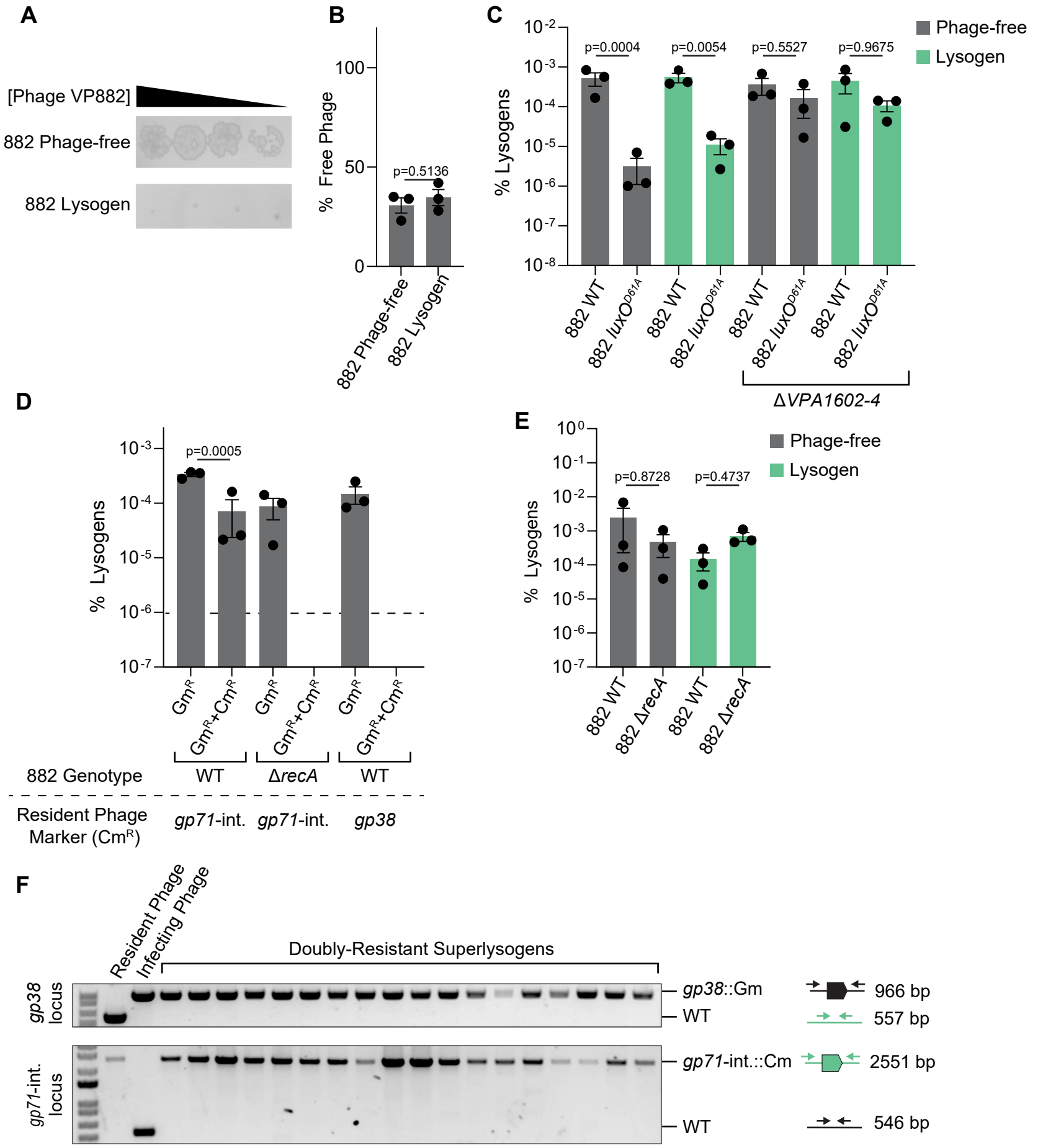
A
[Phage VP882]
882 Phage-free
882 Lysogen
B
% Free Phage
100
50
0
p=0.5136
882 Phage-free
882 Lysogen
C
% Lysogens
Phage-free
Lysogen
p=0.0004
p=0.0054
p=0.5527
p=0.9675
882 WT
882 luxO^D61A
ΔVPA1602-4
D
% Lysogens
p=0.0005
Gm^R
Gm^R+Cm^R
882 Genotype
WT
ΔrecA
Resident Phage Marker (Cm^R)
gp71-int.
gp38
E
% Lysogens
Phage-free
Lysogen
p=0.8728
p=0.4737
882 WT
882 ΔrecA
F
Resident Phage
Infecting Phage
Doubly-Resistant Superlysogens
gp38 locus
gp71-int. locus
gp38::Gm
WT
gp71-int.::Cm
966 bp
557 bp
2551 bp
546 bp

Figure S1

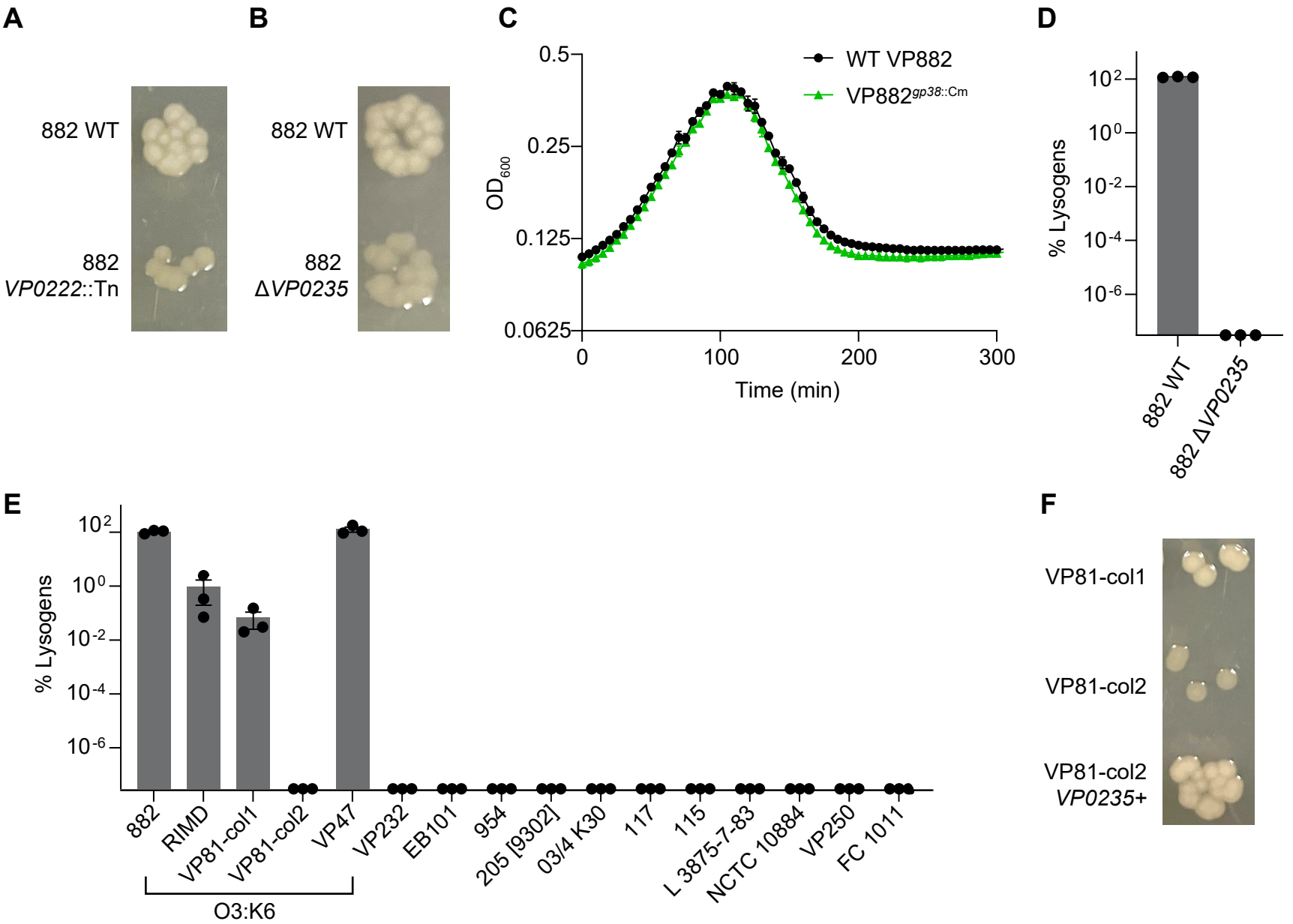
A
882 WT
882
VP0222::Tn
B
882 WT
882
ΔVP0235
C
WT VP882
VP882gp38::Cm
OD600
0.5
0.25
0.125
0.0625
0
100
200
300
Time (min)
D
% Lysogens
10^2
10^0
10^-2
10^-4
10^-6
882 WT
882 ΔVP0235
E
% Lysogens
10^2
10^0
10^-2
10^-4
10^-6
882
RIMD
VP81-col1
VP81-col2
VP47
VP232
EB101
954
205 [9302]
03/4 K30
117
115
L 3875-7-83
NCTC 10884
VP250
FC 1011
O3:K6
F
VP81-col1
VP81-col2
VP81-col2
VP0235+

Figure S2

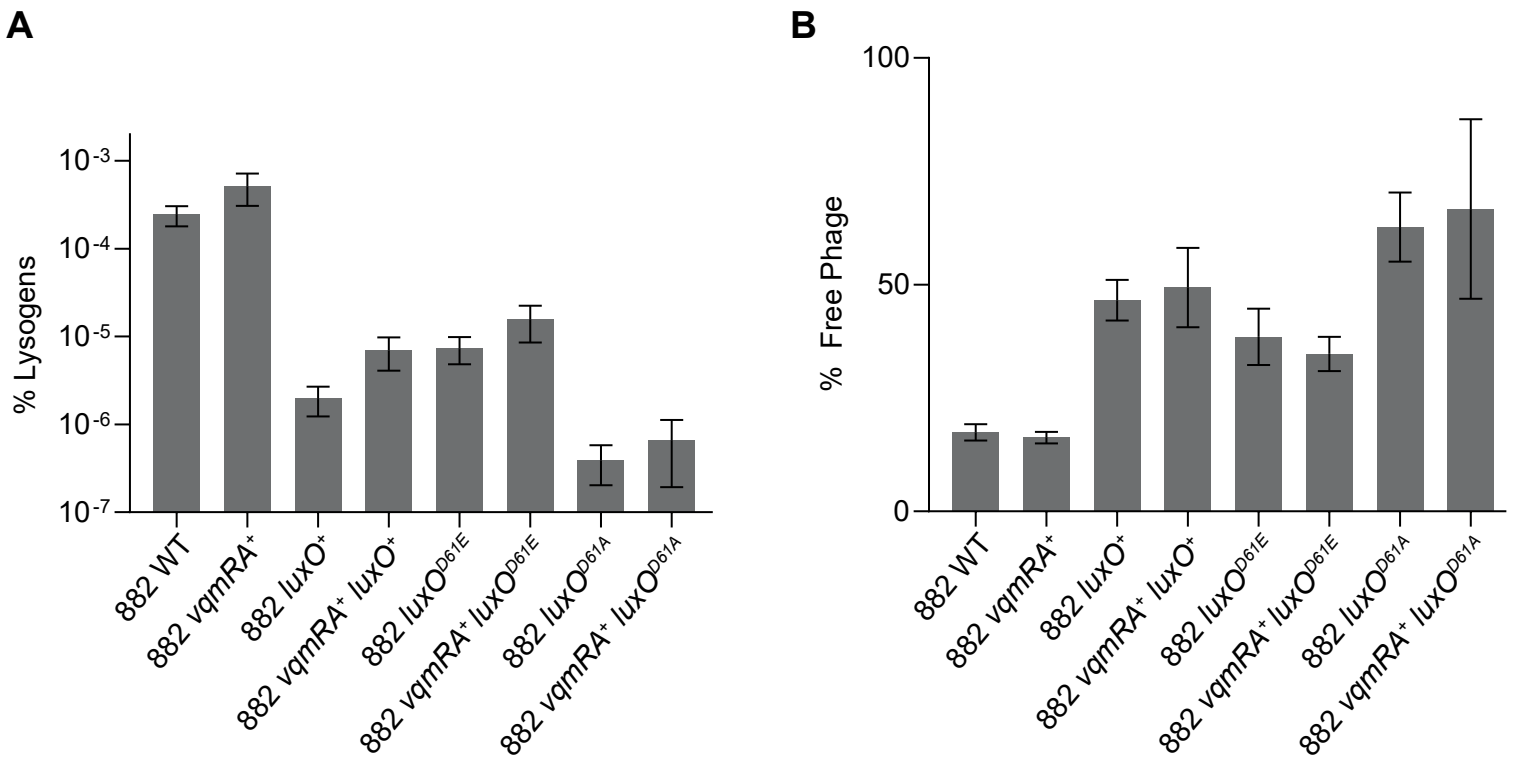
A
% Lysogens
10-3
10-4
10-5
10-6
10-7
882 WT
882 vqmRA+
882 luxO+
882 vqmRA+ luxO+
882 luxOD61E
882 vqmRA+ luxOD61E
882 luxOD61A
882 vqmRA+ luxOD61A
B
% Free Phage
100
50
0
882 WT
882 vqmRA+
882 luxO+
882 vqmRA+ luxO+
882 luxOD61E
882 vqmRA+ luxOD61E
882 luxOD61A
882 vqmRA+ luxOD61A

Figure S3

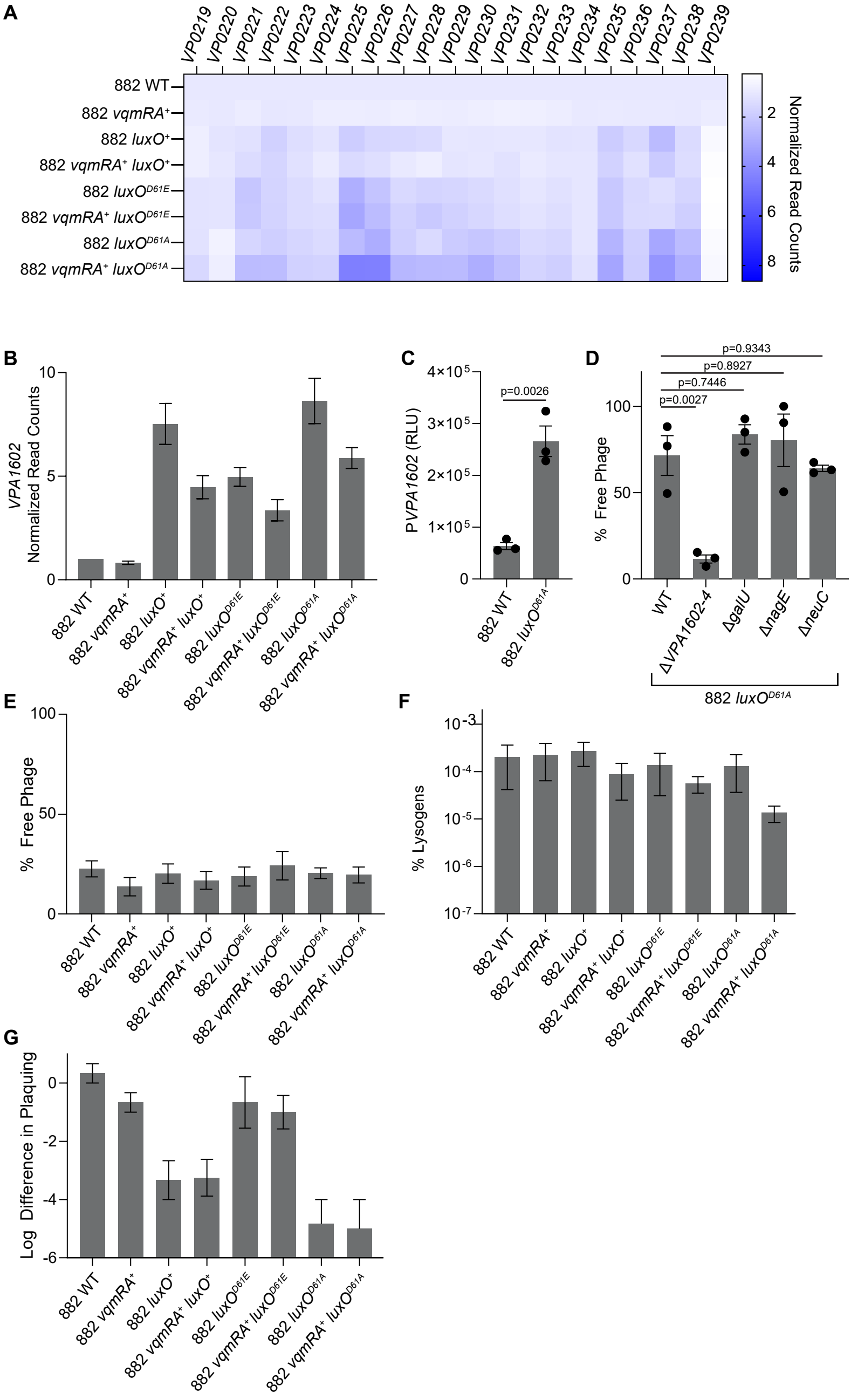
A
VP0219
VP0220
VP0221
VP0222
VP0223
VP0224
VP0225
VP0226
VP0227
VP0228
VP0229
VP0230
VP0231
VP0232
VP0233
VP0234
VP0235
VP0236
VP0237
VP0238
VP0239
882 WT
882 vqmRA+
882 luxO+
882 vqmRA+ luxO+
882 luxOD61E
882 vqmRA+ luxOD61E
882 luxOD61A
882 vqmRA+ luxOD61A
Normalized Read Counts
2
4
6
8
B
VPA1602 Normalized Read Counts
10
5
0
C
PVPA1602 (RLU)
4×10^5
3×10^5
2×10^5
1×10^5
0
p=0.0026
D
% Free Phage
100
50
0
p=0.9343
p=0.8927
p=0.7446
p=0.0027
WT
ΔVPA1602-4
ΔgalU
ΔnagE
ΔneuC
882 luxOD61A
E
% Free Phage
100
50
0
F
% Lysogens
10^-3
10^-4
10^-5
10^-6
10^-7
G
Log Difference in Plaquing
0
-2
-4
-6

Figure S4

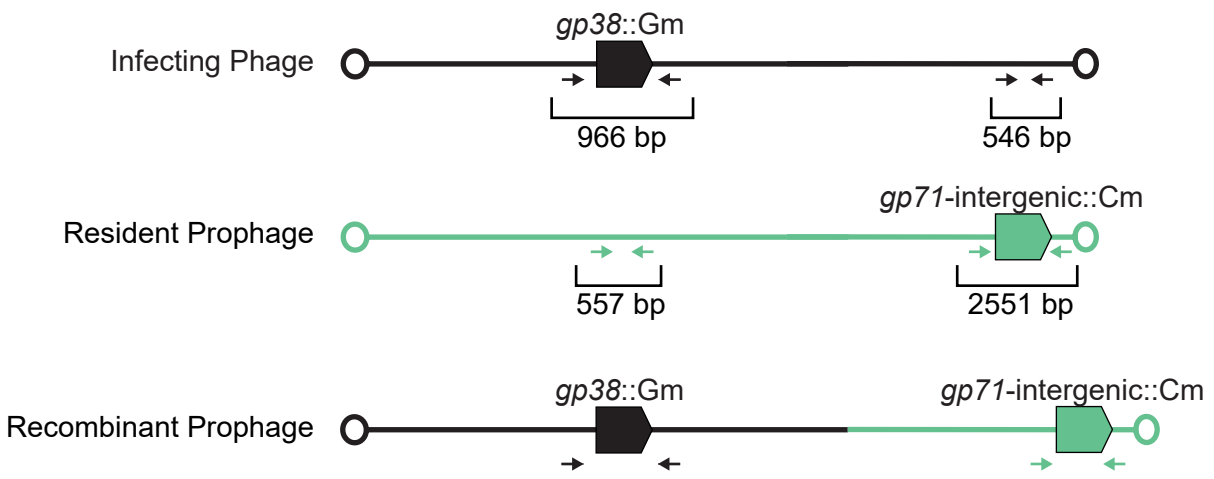
Infecting Phage
gp38::Gm
966 bp
546 bp
Resident Prophage
gp71-intergenic::Cm
557 bp
2551 bp
Recombinant Prophage
gp38::Gm
gp71-intergenic::Cm